Stem Cell Research & Therapy

RESEARCH

Open Access

Metabolic stress and early cell death in photoreceptor precursor cells following retinal transplantation

Raghavi Sudharsan[1*], Natalia Dolgova[1], Jennifer Kwok[1], Alexa Gray[1], Yu Sato[1], Agustin Luz Madrigal[2,7,8], Praveen Joseph Susaimanickam[2,7], Emil Kriukov[3,4], Petr Baranov[3,4], John H. Wolfe[5,6], Gustavo D. Aguirre[1], David M. Gamm[2,7,8] and William A. Beltran[1*]

Abstract

Background Progressive photoreceptor loss in retinal degenerative diseases leads to irreversible vision impairment. Transplantation of human embryonic or induced pluripotent stem cell-derived photoreceptor precursor cells (PRPCs) offers potential for vision restoration. However, substantial early donor cell loss remains a major challenge. This study aims to elucidate the mechanisms underlying early PRPC loss and to evaluate host retinal responses to transplantation.

Methods PRPCs derived from human embryonic stem cells (hESC)-based retinal organoids were subretinally transplanted into both normal and degenerated canine retinas to investigate the impact of host retinal degeneration on transplant survival and integration. Single-cell RNA sequencing (scRNAseq) was performed on transplanted PRPCs 3 days post-transplantation into normal canine retinas, as well as on host retinal cells to identify molecular pathways associated with early donor cell loss. Non-invasive multimodal retinal imaging and immunohistochemical analyses were conducted to assess PRPC survival, integration, and host immune responses.

Results Despite systemic immunosuppression, extensive early loss of human PRPCs occurred within the first week following xenotransplantation into both normal and degenerated canine retinas, suggesting that factors beyond immune activation contribute to donor cell loss. Transcriptomic analysis identified metabolic stress as a key driver of early donor cell death, characterized by dysregulation of mitochondrial function and oxidative phosphorylation pathways. Microglial infiltration into the donor cell mass was also observed in normal retinas, suggesting a response to donor cell stress and apoptosis. Beyond the initial phase of cell death, surviving donor cells integrated and persisted when transplanted into retinas with a partially preserved outer nuclear layer, whereas cell loss continued when intervention occurred at end-stage degeneration.

Conclusions Metabolic stress represents a critical barrier to PRPC survival following transplantation. Strategies aimed at enhancing metabolic resilience may improve transplantation outcomes. Furthermore, host retinal responses shape the transplant microenvironment, influencing donor cell survival and integration. These findings highlight the need

*Correspondence:
Raghavi Sudharsan
raghavi@vet.upenn.edu
William A. Beltran
wbeltran@vet.upenn.edu
Full list of author information is available at the end of the article

for targeted interventions to mitigate early metabolic stress and optimize PRPC transplantation strategies for retinal degenerative diseases.

Keywords Photoreceptor precursor cells, Retinal transplantation, Retinal degenerative diseases, Metabolic stress, Single-cell RNA sequencing

Background

Retinal degenerative diseases, such as age-related macular degeneration (AMD) and retinitis pigmentosa (RP), lead to the progressive loss of photoreceptors, resulting in irreversible vision impairment. Cell-based therapies, particularly transplantation of photoreceptor precursor cells (PRPCs) derived from either embryonic stem cells (ESCs) or induced pluripotent stem cells (iPSCs), have emerged as a promising approach to treat these conditions. These stem cell-derived PRPCs hold the potential to replace lost photoreceptors and restore vision in patients with advanced retinal degeneration. Preclinical studies have shown that ESC- and iPSC-derived PRPCs can survive, integrate, and differentiate into mature photoreceptors within the host retina [1–3]. Notably, even in xenograft models, these precursor cells have demonstrated the ability to integrate into the host retinal architecture and form functional synapses, further supporting their potential to restore visual function [4–6]. The low expression of HLA molecules on the surface of ESC- and iPSC-derived PRPCs along with the retina's status as an immune-privileged site reduces the likelihood of rejection in xenograft settings [7–10]. Nonetheless, successful transplantation of PRPCs still requires effective immunosuppression strategies to minimize the risk of immune rejection, especially for allogeneic and xenogeneic transplants into degenerating retinas where the immune privilege status of the subretinal space is compromised [2, 7, 11, 12].

In our previous work, we established an effective immunosuppression protocol that prevents xenograft rejection and promotes the long-term survival of hESC-PRPCs in both normal and rcd1/*PDE6B* mutant canine retinas when transplanted into the subretinal space. With sustained systemic immunosuppression, we were able to monitor xenograft survival up to 22 weeks post-transplantation. Notably, in mutant retinas, and to a much lesser extent in normal retinas, the transplanted PRPCs migrated into the host retinal cell layers, including the outer and inner nuclear layers (ONL and INL) [2]. This migration is an encouraging sign of potential integration, particularly in the context of studying human stem cell derived PRPC xenograft survival and integration in preclinical models of retinal degeneration.

To further assess the viability of the transplanted cells, we developed a multimodal, non-invasive retinal imaging protocol that combined fundus photography, near-infrared confocal scanning laser ophthalmoscopy (cSLO), and *en-face* spectral-domain optical coherence tomography (OCT) imaging [2]. This approach allowed for real-time monitoring of PRPC survival in the subretinal space, providing valuable insight into the dynamics of graft integration. While these imaging techniques proved to be effective for long-term monitoring, they also revealed an important challenge in the early phases of transplantation. Specifically, between 3 days and 1-week post-transplantation, we observed a significant loss of transplanted PRPCs in immunosuppressed animals [2]. Although no further cell loss occurred beyond the first week, this early depletion of transplanted cells limited the number of surviving PRPCs available for subsequent integration and long-term survival and function. The early cell death, which has been noted in other studies, represents a critical bottleneck in the success of cell-based therapies for retinal degenerative diseases [13, 14].

Innate immune responses [15], cellular damage during retinal organoid (RO) fragmentation and/or subretinal injection [16], as well as anoikis [17]—apoptosis triggered by the loss of cellular adhesion—have all been proposed as potential causes for early donor cell loss following transplantation. Anoikis may be mitigated by transplanting retinal fragments/aggregates instead of a single-cell suspension [18], an approach we employed in our previous study [2]. While activated microglia infiltrate the ONL and the subretinal space in degenerated retinas, where they can access the transplanted cell mass, this is not observed in normal retinas. Nonetheless, early donor cell death occurs in both degenerated and normal retinas following transplantation, indicating that other mechanisms may be at play.

In this study, we examined the molecular and cellular mechanisms underlying early donor cell death within the first week post-transplantation. We used a transcriptomic approach that provided a comprehensive understanding of the molecular events leading to the loss of transplanted PRPCs and identified key pathways that could be targeted to improve cell survival. Additionally, we extended our investigation to two additional canine models of retinal degeneration at different disease stages to determine whether early transplant loss is influenced by the underlying retinal pathology and/or the stage of degeneration. It is important to note that while we use

the term PRPCs throughout this study, the transplanted cells originate from hESC-derived ROs, which predominantly consist of PRPCs and differentiated photoreceptors, along with other retinal cell types [2, 19–21]. Our findings revealed metabolic stress as a critical factor that significantly impacts the survival of PRPCs immediately following subretinal transplantation.

Methods

All protocols, including the research question, key design features, and analysis plan, were developed prior to the study but were not formally registered. The work has been reported in line with the ARRIVE guidelines 2.0.

Study animals: The dogs utilized in this study were bred and housed under identical conditions (diet, ambient illumination with cyclic 12 h ON-12 h OFF light) at the University of Pennsylvania's Retinal Disease Studies Facility. All procedures complied with the ARVO Statement for the Use of Animals in Ophthalmic and Vision Research and were approved by the Institutional Animal Care and Use Committee (IACUC) at the University of Pennsylvania. A detailed summary of the study animals and the procedures performed is provided in Table 1.

Immunosuppression protocol: Dogs received a combined immunosuppressive regimen starting 1 week prior to cell transplantation and continuing throughout the study, as previously described [2]. Oral cyclosporine A (CsA) was administered at 5 mg/kg in the morning and 10 mg/kg in the evening, delivered in a small food bolus, separate from full meals. Oral mycophenolate mofetil (MMF) was given at 10 mg/kg twice daily in liquid form without food. Oral prednisolone was initiated on the day of transplantation at 1 mg/kg once daily and tapered to 0.1 mg/kg over 12 weeks post-injection. Topical corticosteroid treatment included prednisolone acetate administered from the day of transplantation through 4 weeks post-injection and dexamethasone on the day of surgery. Subconjunctival triamcinolone acetonide (4 mg) was administered at the time of transplantation and repeated at week 4. Systemic immunosuppression was monitored via pharmacokinetic and pharmacodynamic testing of blood cyclosporine levels at 1 week post-injection and every 4 weeks thereafter.

Preparation of PRPCs for subretinal transplantation and culture: Three-dimensional ROs were generated from the WA09 *CRX*$^{+/tdTomato}$ hESC reporter line (University of Wisconsin) to produce fluorescently labeled PRPCs using established protocols [19, 21, 22]. The ROs were shipped overnight to the University of Pennsylvania in transport medium containing Hibernate CTS supplemented with 2% FBS, 2% B27 and 1% PSA maintained at 4 °C. Upon arrival, the ROs were transferred to retinal differentiation medium (RDM) supplemented with retinoic acid and 2% FBS and maintained in a 5% CO_2 incubator. Cells were cultured in this media for up to 1 week prior to transplantation, with media changes occurring every 2–3 days. To prepare for transplantation, ROs were washed multiple times with Hank's Balanced Salt Solution (HBSS, without calcium and magnesium) and mechanically triturated to generate PRPC-rich fragments. These fragments were not sorted or enriched based on CRX-driven tdTomato fluorescence and therefore contained a heterogeneous mixture of retinal cell types present within the organoids. These fragments were then transplanted subretinally into normal or mutant dogs at various stages of retinal degeneration [23–25] using a previously described 5-step surgical approach and a custom-modified subretinal injector [2]. For scRNAseq experiments, approximately 8–10 million cells were transplanted per eye, while about 2 million cells were maintained as fragments in culture in RDM for 3 days. The final volume of cell suspension injected subretinally varied slightly between animals and was determined at the time of surgery based on the observed distribution of cells within the subretinal space versus any reflux into the vitreous cavity. The surgical goal was to maximize the number of cells delivered into the subretinal compartment.

Non-invasive multimodal retinal imaging of the transplanted cells: Live imaging of the transplanted cells at timepoints listed in Table 1 was performed as previously described [2] using a retinal camera (TRC-50Ex, TopCon Medical Systems, Paramus, NJ, USA) that was modified to enable detection of tdTomato fluorescence, and a cSLO/OCT unit (Spectralis HRA/OCT2 unit, Heidelberg Engineering, Heidelberg, Germany).

Processing of cultured and transplanted RO fragments and host retinal tissue, library preparation and scRNAseq: At termination, dogs were humanely euthanized in accordance with the AVMA 2020 guidelines using an intravenous overdose of pentobarbital sodium and phenytoin sodium (Euthasol; Virbac, Westlake, TX, USA; 200 mg/kg). Death was confirmed by the absence of a pulse and respiration, as well as the inability to detect respiratory sounds or a heartbeat using a stethoscope. Eye cups were separated from the anterior segment, vitreous removed and 3 mm-diameter biopsies of host neuroretina within and outside of areas of xenotransplantation were collected with disposable biopsy punches. In areas of xenotransplantation where the host neuroretina was biopsied, transplanted PRPC-rich fragments of ROs present in the subretinal space were then collected with an Elschnig cyclodialysis spatula. Cultured and transplanted PRPC-rich fragments were dissociated into single cells using the Miltenyi Biotec Neural Tissue Dissociation kit—Postnatal Neurons (Cat. No. 130–094-802, Miltenyi

Table 1 Details of cell transplantation and monitoring time-points in all study animals

Genotype (disease)	Dog ID (sex, age in weeks at injection)	Eye	Rows of nuclei in ONL at dosing*	Cell suspension type	Estimation of cells delivered in the SRS	Donor cells age at transplantation	Day1	Day2	Day3	1 w*	4 w*	8 w*	12 w*	16 w*	20 w*	31 w*
$RHO^{T4R/+}$ (Light damage)	EM543 (F, 130)	OS	~1	Frag. *CRX*$^{+/}$ tdTomato	8 million in 50 µL	105 112 147	LI		LI	LI	LI					
	EM401 (F, 365)	OS	~1	Frag. *CRX*$^{+/}$ tdTomato	8 million in 50 µL	140 169	LI			LI	LI	LI	LI			
	EM421 (M, 339)	OS	~1	Frag. *CRX*$^{+/}$ tdTomato	8 million in 50 µL	121	LI			LI	LI	LI	LI			
	EM469 (F, 238)	OS	~1	Frag. *CRX*$^{+/}$ tdTomato	8 million in 50 µL	121	LI			LI	LI	LI	LI	LI	LI	LI
Mutant RPGR (XLRP)	Z710 (M, 88)	OS	~1	Frag. *CRX*$^{+/}$ tdTomato	8 million in 70 µL	140	LI			LI	LI	LI	LI			
	Z720 (M, 43)	OS	~3	Frag. *CRX*$^{+/}$ tdTomato	6.7 million in 50 µL	127	LI			LI	LI	LI	LI	LI	LI/IHC	
Normal	LG5 (F, 66)	OD	~10	Frag. *CRX*$^{+/}$ tdTomato	10 million in 100 µL	122 126	LI	LI	scRNAseq							
		OS		Frag. *CRX*$^{+/}$ tdTomato	11 million in 110 µL	122 126	LI	LI	IHC							
	RC726 (M, 50)	OD	~10	Frag. *CRX*$^{+/}$ tdTomato	10 million in 100 µL	113 120	LI	LI	IHC							
		OS		Frag. *CRX*$^{+/}$ tdTomato	10 million in 100 µL	113 120	LI	LI	scRNAseq							
	RC724 (M, 63)	OD	~10	Frag. *CRX*$^{+/}$ tdTomato	8 million in 50 µL	117	LI	LI	IHC							
		OS		Frag. *CRX*$^{+/}$ tdTomato	8 million in 50 µL	117	LI	LI	scRNAseq							

OD: right eye; OS: left eye; *: estimated based on published disease characterization studies [23–25]; Frag.: fragmented; SRS: subretinal space; Day1: immediately post transplantation; w*: weeks post transplantation ± 1 week; LI: live imaging; IHC: immunohistochemical assessment; scRNAseq: single cell RNA sequencing

Biotec, Inc., Auburn, CA, USA) following manufacturer's protocol. Canine retinal tissues were first incubated in 0.25% Trypsin at 37 °C for 10 min, then dissociated into single cells using the same dissociation kit. Following dissociation, cell counts were determined by automated counting with the Luna-FL dual fluorescence cell counter. For each sample, 10,000 cells were loaded onto the 10X Genomics Chromium Next GEM Chip G. Library preparation was performed using the Chromium Next GEM Single Cell 3' kit v3.1 (10 × Genomics, Pleasanton, CA, USA). The libraries were pooled and sequenced on an Illumina Novaseq 2000 platform (Illumina, San Diego, CA, USA) at the PennVet Center for Host Microbial Interactions (CHMI) core laboratory.

Analysis of scRNAseq data: Single-cell RNA sequencing data were processed using the Cell Ranger (v7) pipeline (10 × Genomics) to generate gene expression matrices. Sequencing reads were aligned to the human (GRCh38) or canine (CanFam6) reference genome, as appropriate, using the STAR algorithm within Cell Ranger. Quality control, data normalization, clustering, and downstream analyses were performed in R using the Seurat v.4 package [26, 27]. After excluding cells with low gene counts (< 200 genes per cell), high mitochondrial gene content (> 5%), or high gene count outliers, the remaining cells were normalized using the SCTransform method.

To assess potential contamination from host canine cells in the transplanted PRPC preparations, sequencing reads were also aligned to a combined reference genome that included both human (GRCh38) and canine (CanFam6) transcriptomes, with gene names prefixed with *hsa-* or *cfa-* to distinguish species of origin. Cells were classified as human, canine, or mixed based on the proportion of species-specific transcripts. This analysis was performed independently for all three scRNAseq experiments, with each showing similar species classification patterns. For clarity, results from one representative replicate are presented in the Results section. Importantly, all downstream analyses described in this study were conducted exclusively on filtered expression matrices generated using alignment to the human genome alone, ensuring that only human donor cells were included.

Experimental repeats were integrated using Seurat's PrepSCTIntegration, FindIntegrationAnchors, and IntegrateData functions to remove batch effects. Principal component analysis (PCA) was performed on the integrated dataset, followed by UMAP for dimensionality reduction. Clusters were annotated based on the expression of known cell type-specific markers. Differential gene expression analysis between experimental conditions or clusters was performed using Seurat's FindMarkers function. Significant genes (adjusted p-value < 0.05) were identified and used for pathway analysis. Ingenuity Pathway Analysis (IPA, Qiagen) was used to identify canonical pathways and biological functions enriched in the dataset, with pathways having a Benjamini–Hochberg adjusted p-value < 0.05 considered significant.

Cell fate trajectory inference with RNA Velocity: Raw .bam files generated from Cell Ranger were processed into.loom files using samtools [28] and velocyto v.0.17.17 [29]. These.loom files were then concatenated using the built-in Scanpy function. Prior to concatenation, individual scRNA-seq datasets in .h5Seurat format were converted to .h5ad format using SeuratDisk. Downstream analysis, including RNA velocity and trajectory inference, was performed using scVelo in a Python v.3.12-based environment.

Dissociation and culture of retinal organoids for immunohistochemistry: Stage 2 retinal organoids derived from the WA09 *CRX*$^{+/tdTomato}$ line were dissociated into single cells and cultured for immunohistochemistry. Organoids were washed in calcium- and magnesium-free DPBS and incubated in 10X TrypLE Select (Thermo Fisher Scientific) at 37°C for 30–35 min with intermittent trituration. Dissociation was quenched using a solution of DNase I (0.05 mg/mL final; STEMCELL Technologies, Vancouver, Canada) in retinal differentiation medium [RDM; 3.5:1.5 DMEM: F12 (Gibco, Thermo Fisher Scientific, USA), 1× Antibiotic–Antimycotic (Gibco), 1× GlutaMAX™ (Gibco)] supplemented with retinoic acid and ROCK inhibitor. Cells were filtered through a pre-wetted 30 µm MACS SmartStrainer (Miltenyi Biotec), pelleted by centrifugation, and resuspended in 3D-RDM [3.5:1.5 DMEM:F12, 2% B27 supplement, 1× GlutaMAX, 5% FBS (WiCell, Madison, WI, USA), 100uM taurine (Sigma-Aldrich, St. Louis, MO, USA), and 0.4% [v/v] Chemically Defined Lipid Concentrate (Gibco) + ROCK inhibitor. After counting, 100,000 viable cells were plated per well onto 8-well chamber slides pre-coated with Laminin-111 (1:20 dilution in DMEM-F12; Fisher Scientific) and cultured at 37°C in 5% CO_2. Media was partially replaced the next day. The cells were maintained for 3 days prior to fixation (4% paraformaldehyde for 15 min at room temperature) and immunohistochemistry.

Tissue preparation for immunohistochemistry: Following euthanasia, eyes from four dogs (Table 1) were enucleated and fixed in 4 or 2% paraformaldehyde (PFA), cryoprotected in sucrose, and embedded in OCT compound as previously described (29). Retinal cryosections (10 µm thickness) were collected onto Superfrost Plus slides and stored at −20°C until use.

Immunohistochemical analysis: For both retinal cryosections and dissociated PRPCs cultured on chamber slides, immunohistochemistry was performed using

standard protocols. Samples were permeabilized with 0.25% Triton X-100 in PBS and blocked in solution containing 5% bovine serum albumin (BSA) and 4.5% fish gelatin in PBS. Primary antibodies (listed in Supplementary Table 1) were applied in blocking buffer and incubated overnight at 4 °C. The following day, samples were incubated with Alexa Fluor-conjugated secondary antibodies (Invitrogen, Thermo Fisher Scientific) and counterstained using Hoechst 33,342 (Thermo Fisher Scientific) to visualize nuclei. The immunolabeled sections were examined using a Leica TCS SP5 confocal microscope (Leica Microsystems, Buffalo Grove, IL, USA). Images were acquired and processed with the Leica Application Suite and then prepared for display using Adobe Photoshop and Illustrator.

LIVE/DEAD cell viability assay: Stage 2 retinal organoids were subjected to mechanical trituration as described for transplantation. Cells were incubated with the Live/Dead Fixable Green Dead Cell Stain Kit (Thermo Fisher Scientific) following manufacturer's instructions. Fluorescent images were acquired using an epifluorescence microscope (Axioplan, Carl Zeiss Meditec, Oberkochen, Germany) and analyzed with Fiji software [30]. For each condition, ten fields were imaged and quantified. Hoechst-positive nuclei were counted to determine total cell number, and green fluorescent signal indicated dead cells. The number and percentage of dead cells were calculated and compiled in Excel for comparative analysis.

Results

Acute loss of hESC-PRPCs following transplantation is associated with limited migration and structural integration into the host ONL

We previously demonstrated that subretinally injected tdTomato-labeled PRPCs, derived from a WA09 *CRX*$^{+/tdTomato}$ hESC [21] line, survive long term in immunosuppressed normal canine retinas (n = 4 dogs). Donor cells remained detectable for up to 22 weeks post-injection, primarily within the subretinal space, with occasional migration into the host ONL. A subset of cells exhibited cone-like morphology, suggesting early photoreceptor differentiation. In contrast, when PRPCs were transplanted into rcd1/*PDE6B* dogs at a late stage of degeneration (~ 2 ONL rows remaining), migration was more frequent but disorganized, with cells localizing to both the ONL and inner retina. These donor cells did not adopt photoreceptor-like features, underscoring the negative impact of structural alterations in end stage disease on PRPC integration and maturation [2].

To assess how disease type and/or the stage (degree of ONL loss) at the time of transplantation could influence PRPC fate, we conducted similar experiments in two additional non-allelic canine models at different stages of retinal degeneration. Across all four models -normal, rcd1/*PDE6B*, *RHO*$^{T4R/+}$, and xlpra2/*RPGR* - we observed substantial loss of tdTomato fluorescence within the first week post-transplantation (Fig. 1). Since the outcomes in normal and rcd1/*PDE6B* retinas have been previously characterized [2], the current study focuses on the *RHO*$^{T4R/+}$ and xlpra2/*RPGR* models to further evaluate how disease severity influences long-term donor cell survival and integration. First, we assessed the survival of PRPCs following subretinal injection into mutant *RHO*$^{T4R/+}$ dogs at end stage retinal degeneration, where only a single row of cone nuclei remained in the ONL. These dogs had previously been acutely exposed to light levels that trigger rapid and complete loss of rods in the central to mid-peripheral retina [24, 25]. Fundus fluorescence photography revealed qualitatively a significant reduction in tdTomato fluorescence within the first week following injection in all 4 injected *RHO*$^{T4R/+}$dogs (four eyes). Notably, in contrast to the findings in normal and rcd1/*PDE6B* dogs [2], further reduction in tdTomato signal was observed in three out of four *RHO*$^{T4R/+}$ animals despite uniform immunosuppressive regimen (Fig. 1c–f). A similar continuous decline in tdTomato fluorescence was also noted in one xlpra2/*RPGR* mutant dog injected at 88 weeks of age, when retinal degeneration was at end-stage disease (~ one row of nuclei remaining in the ONL) (Fig. 1g). To determine whether this fluorescence loss reflected true donor cell clearance, we performed endpoint histological and immunohistochemical analysis in all animals. Staining for human nuclear marker Ku80 along with visualization of tdTomato confirmed complete loss of donor cells in three of the four *RHO*$^{T4R/+}$ dogs and in the xlpra2/*RPGR* dog injected at end stage. In one *RHO*$^{T4R/+}$ dog (EM401), a small number of surviving PRPCs were detected localized to the subretinal space (Supplementary Fig. 1A–E). These results suggest that the retinal environment in end-stage disease may not be conducive to the long-term survival of transplanted cells.

To assess whether transplantation at a less advanced stage of photoreceptor degeneration (~ three rows of nuclei left in the ONL or late-stage degeneration) would promote long-term survival of PRPCs, a 43-week-old xlpra2/*RPGR* dog was injected and followed for up to 22 weeks post-injection (PI). A significant loss of cells occurred within the first week PI, however more tdTomato fluorescence was observed throughout the treated area and was stable on in vivo imaging up to 20 weeks PI, the final imaging timepoint before termination at 22 weeks for histological analysis (Fig. 1h). Upon termination, histological and immunohistochemical assessment confirmed the presence of tdTomato-positive PRPC foci distributed throughout the treated/bleb area. These

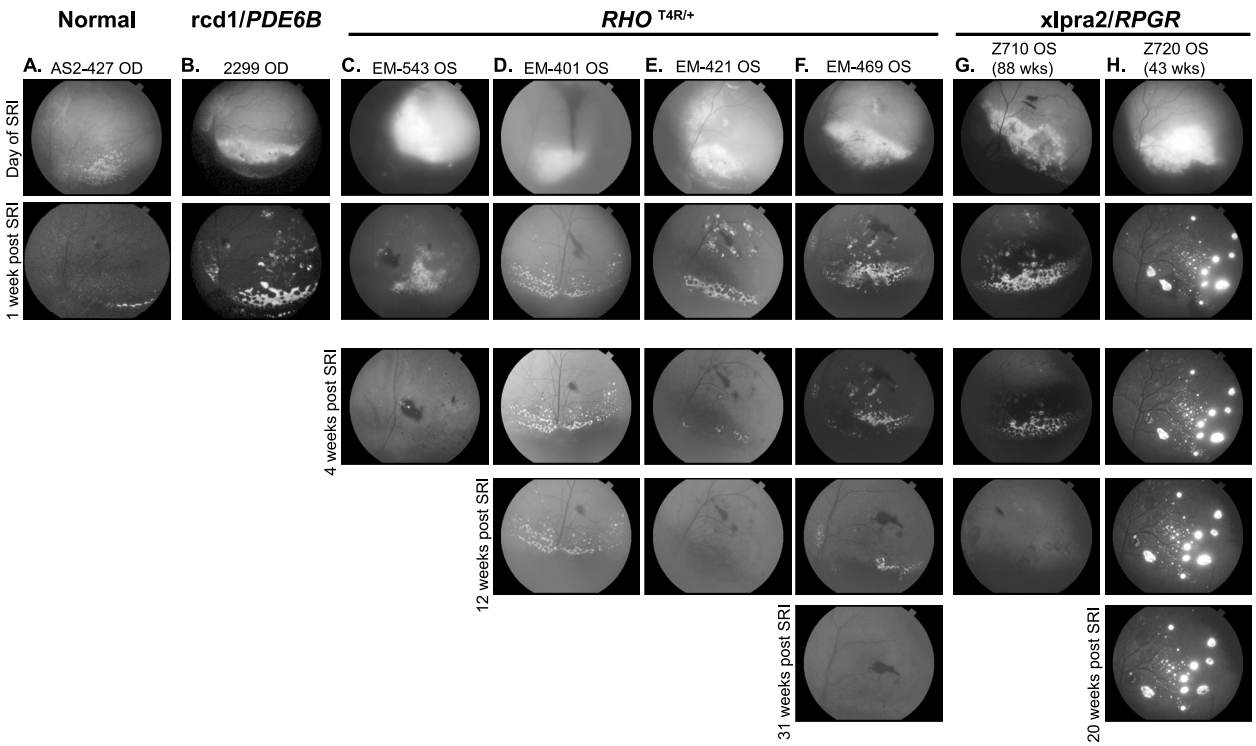

Fig. 1 Retinal imaging following subretinal transplantation of hESC-CRX$^{+/tdTomato}$-derived photoreceptor precursor cells (PRPCs) following subretinal transplantation in canine models of retinal degeneration. Fundus fluorescence images of tdTomato-expressing PRPCs at early and extended time points post-transplantation. **a–b** Early imaging of grafts in (**a**) Normal (AS2-427) and (**b**) rcd1/*PDE6B* (2299) retina, immediately following subretinal injection and 1 week later. Both animals were included in our previous study (Ripolles-Garcia et al., 2022); however, the images shown here have not been published previously. **c–h** Longitudinal imaging of tdTomato^{+} grafts in RHO$^{T4R/+}$ and xlpra2/*RPGR* dogs at multiple time points following subretinal injection, in animals with end-stage **c–g** and late-stage (**h**) retinal degeneration. All animals received systemic immunosuppression. In panel **g**, the dark shading in the inferior fundus on the day of injection is due to normal pigmentation of the retina and not indicative of hemorrhage; the surrounding gray area corresponds to the retinal detachment caused by the injection bleb. This image was acquired using low flash intensity due to the brightness of the tdTomato signal

cells were predominantly localized either within the subretinal space or had migrated into the host retina, though in a disorganized pattern (Supplementary Fig. 1F). Interestingly, at a single locus, PRPCs that had differentiated predominantly into cones were found to be perfectly aligned in the host's ONL, immediately below the external limiting membrane. These cells formed a short inner segment and extended a short axon with pedicle-like synaptic terminals (Fig. 2). Notably, immunostaining for RPE65 in adjacent sections confirmed that these cells were integrated beneath the ELM and not merely apposed to the RPE, supporting true structural integration into the host retina (Fig. 2C2).

Taken together, these findings suggest that the persistence of at least three rows of nuclei in the host's ONL may provide a more favorable environment for donor PRPCs, supporting their long-term survival and enabling a subset to differentiate into radially elongated photoreceptors. However, even at this less advanced stage of disease, the substantial early loss of donor cells following transplantation may account for the limited occurrence of successful integration events.

Three days after subretinal injection, transplanted hESC-PRPCs exhibit similar cell cluster profiles as cultured cells

To investigate the factors contributing to the prominent early death of PRPCs after transplantation into the canine subretinal space, we conducted single-cell RNA sequencing (scRNAseq) on transplanted PRPCs. Approximately 10 million cells from stage 2 ROs (day 110–126) developed from hESC-derived WA09 *CRX*$^{+/tdTomato}$ line [21] were triturated into fragments and injected subretinally into systemically immunosuppressed healthy wild-type canine retinas. To evaluate whether mechanical dissociation itself compromised donor cell viability, we performed a LIVE/DEAD assay comparing RO cells before and after trituration. The results demonstrated no significant increase in cell death following dissociation (Supplementary Fig. 2),

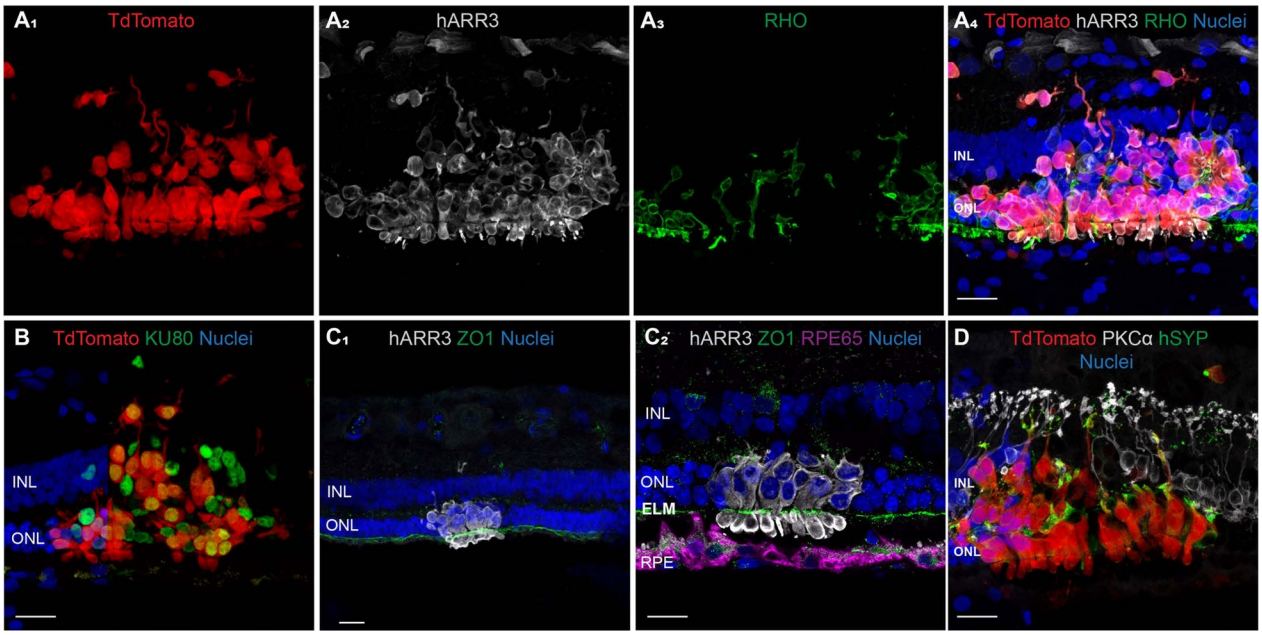

Fig. 2 Differentiation, migration, and synapse formation after transplantation of donor human PRPCs in the xlpra2/*RPGR* host retina at late-stage disease. Immunohistochemical analysis of a site of integration of human PRPCs 20 weeks post transplantation in a 43-week-old mutant xlpra2/*RPGR* dog (ID: Z720). **A**$_{1-4}$ tdTomato-positive human PRPCs primarily differentiated into cone-arrestin (hARR3)-positive photoreceptors located into the host outer nuclear layer (ONL) and inner nuclear layer (INL). **B** All tdtomato-positive cells express human nuclear antigen (Ku80) confirming they are transplanted cells of human origin. Apparent tdTomato^{+}/Ku80^{-} signals reflect cytoplasmic extensions from donor cells overlying host nuclei, as confirmed by inspection of individual confocal z-sections. **C**$_{1-2}$ Reconstitution of a continuous ZO1-positive external limiting membrane (ELM) after migration of human cone arrestin (hARR3)-positive PRPCs into the canine (host) ONL. **D** Transplanted PRPCs express human synaptophysin at their terminals and establish contacts with the host rod bipolar cells. (PKCα-positive). Scale bar = 20 µms

indicating that the observed cell stress and death in transplanted PRPCs cannot be attributed to preparative artifacts alone. Transplanted cell aggregates were visualized using optical coherence tomography (OCT) imaging 2 days PI (Fig. 3a), and harvested the following day (3 days PI) for scRNAseq analysis. This early time point was selected to maximize recovery of viable transplanted cells and enable identification of early markers associated with impending cell stress or death. For comparison, cells from the same batch of ROs were processed through dissociation but maintained in vitro for 3 days, allowing us to control for the effects of mechanical dissociation. To mitigate variability across batches, three independent transplantation experiments were performed.

To confirm that the analyzed cells originated exclusively from the transplanted human PRPCs and were not contaminated with host canine tissue, we aligned the same sequencing data to a combined human-canine reference genome and examined species-specific transcript expression. In one representative experiment, 11,022 cells were identified using the combined reference, of which 7,886 (71.5%) were classified as human, 6 (0.05%) as canine, and 3,121 (28.3%) as mixed, based on transcript content. Comparison with the human-only alignment revealed 7,336 total cells, with 6,426 barcodes (87.6%) overlapping between the two alignments. Similar distributions of species classification were observed in the two additional biological replicates. The presence of a small "mixed" population, including in samples

(See figure on next page.)

Fig. 3 Single cell RNA sequencing (scRNAseq) analysis of donor PRPCs: **a** Near-Infrared cSLO image and single OCT b-scan showing the localization of subretinally-injected PRPCs (white asterisk) within the host retina two days post-transplantation. Green arrow indicates the location of OCT b-scan. **b** Schematic representation of the experimental workflow for isolating donor PRPCs and host retinal tissue for scRNAseq analysis. Created in BioRender. **c** UMAP plot illustrating major cell types identified in cultured and transplanted donor PRPCs. **d** Dot plot displaying key marker genes used for annotating cell clusters. **e** Proportions of each cell type identified in cultured versus transplanted PRPCs, derived from three independent experiments [mean (SD)]

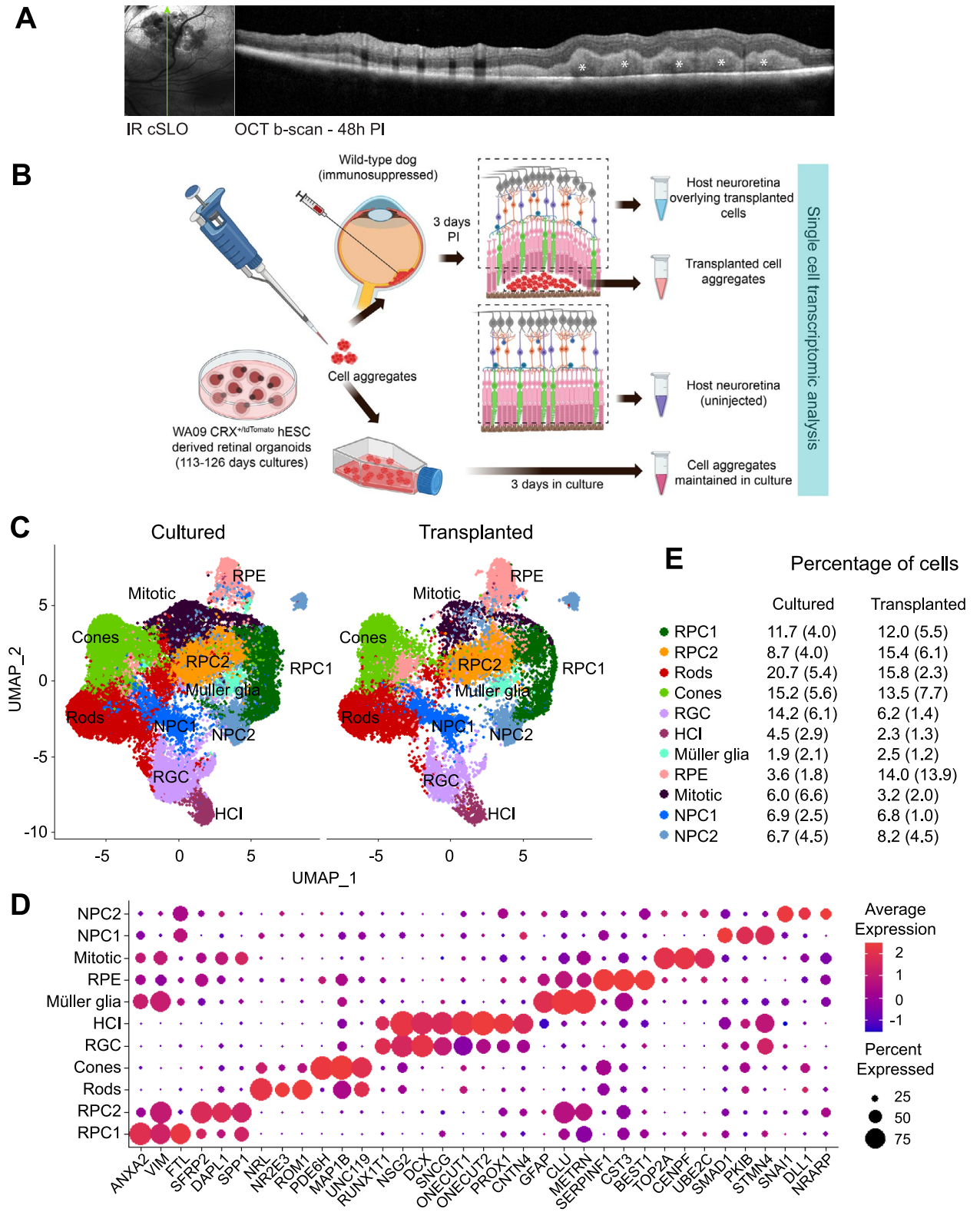

Fig. 3 (See legend on previous page.)

cultured exclusively in vitro, suggests technical artifacts such as alignment to homologous sequences rather than true cross-species contamination. Importantly, all downstream analyses in this study were performed exclusively on cells aligned to the human genome alone, ensuring that only human donor cells were analyzed.

Additionally, we analyzed cells from the host canine retinas, comparing regions directly overlying the transplanted cells with regions where no PRPCs were present. The full study design is summarized in Fig. 3b. A total of 17,715 transplanted and 34,034 cultured cells were analyzed, leading to the identification and annotation of several retinal cell clusters, including rods, cones, horizontal cells and interneurons (HCIs), retinal ganglion cells (RGCs), retinal pigment epithelium cells (RPEs), Müller glia (MG), mitotic cells (MC), two distinct clusters of retinal progenitor cells (RPCs), and two clusters of neural progenitor cells (NPCs) (Fig. 3c). The cell clusters were assigned based on expression of groups of specific marker genes in the clusters (Fig. 3d). The percentage distribution of cells across these clusters showed no significant differences between the cultured organoids and transplanted cell microaggregates, however variability in cell numbers was noted across the three experiments (Fig. 3e). Notably, the percentage of RPE cells appeared elevated in the transplanted samples (14 vs. 3.6%). While this difference was not statistically significant, it may reflect subtle differences in RPE survival, enrichment, or early integration behavior in vivo and warrants further investigation. Overall, these findings align with our expectations, as no substantial differences in cell differentiation between cultured and transplanted cells were anticipated within the initial 3 days post-transplantation and batch-to-batch variability between retinal organoids has been noted earlier [19].

RNA velocity analysis reveals dynamic transcriptional trajectories in rods and cones during culture and following transplantation

While the proportional distribution of cell types remained consistent between cultured and transplanted conditions at this early time point, we sought to investigate dynamic transcriptional changes within specific cell types during culture and transplantation. To this end, RNA velocity [29] analysis was performed to reconstruct transcriptional trajectories and assess maturation states in rod and cone photoreceptors. The analysis revealed dynamic transcriptional changes in rod and cone photoreceptors during differentiation in culture and following transplantation. ForceAtlas2-based [31] embedding of cone and rod populations (Fig. 4a–b, respectively) demonstrated a single trajectory of maturation under both cultured and transplanted conditions. However, RNA velocity vectors uncovered distinct dynamic differences between conditions and between the two photoreceptor types (Fig. 4c–d). In cones, RNA velocity vectors in the cultured condition pointed toward immature states, indicating a reduced commitment to maturation. Conversely, in the transplanted condition, vectors pointed toward maturation, with longer vectors observed in mature cells. This suggests enhanced transcriptional activity and a potential adaptive response to transplantation, allowing for greater functional integration in the host retina (Fig. 4c). In rods, transcriptional activity consistently pointed toward maturation under both conditions. Shorter RNA velocity vectors in mature cells in the cultured condition reflected reduced transcriptional activity, indicative of stabilization at terminal differentiation. In the transplanted condition, mature rods exhibited longer RNA velocity vectors, suggesting elevated transcriptional activity possibly due to adaptive responses to transplantation, efforts to integrate into the host retina, or activation of repair pathways (Fig. 4d).

Heatmaps (Fig. 4e–h) further illustrated gene expression dynamics during photoreceptor maturation via unsupervised clustering of variable genes along transcriptional trajectories. In cultured cones, gene expression profiles showed a progression from genes associated with neuronal plasticity, transcriptional regulation, and stress responses (e.g., GAP43, CDKN1A, MEF2D, NFIA, USP48) to those involved in terminal differentiation, metabolism, and membrane dynamics (e.g., GUCA1B, GAD2, STMN2, GNAT2, DCX), indicative of increasing functional and synaptic maturity. Similarly, in rods, the gene expression profiles (e.g., RCVRN, GNGT1, RP1, IMPG1, PTPRZ1) demonstrated a transcriptional commitment to functional and synaptic maturation. In the transplanted condition, both rods and cones exhibited

(See figure on next page.)

Fig. 4 Continuous transcriptomic changes in human stem-cell derived cone and rod photoreceptors before and after transplantation: **a–b** ForceAtlas diagrams showing the integration of cultured and transplanted cone (**a**) and rod (**b**) photoreceptor subsets, illustrating full overlap of transcriptional states across conditions. **c–d** RNA velocity inferred trajectories for respectively cultured and transplanted cones (**c**) and rods (**d**), with arrows indicating the direction and velocity of transcriptional changes for each individual cell. **e–h** RNA velocity-based heatmaps highlighting variable genes along the transcriptional trajectories for cultured cones (**e**), transplanted cones (**f**), cultured rods (**g**) and transplanted rods (**h**), illustrating the progression of gene expression dynamics across maturation process

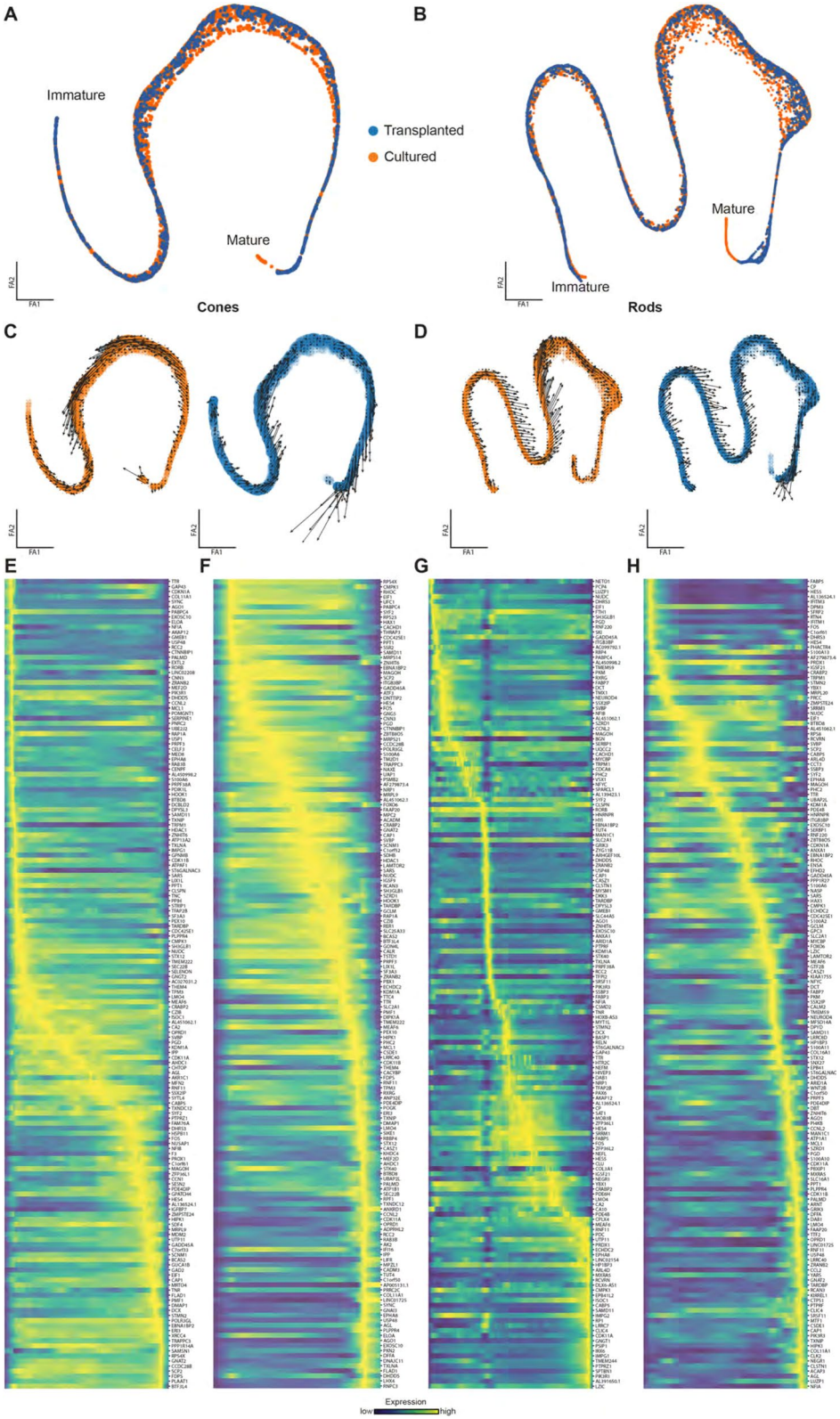

Fig. 4 (See legend on previous page.)

stress-related genes (GADD45A, CCL2, IFITM3, TXNIP etc.) alongside markers of cellular and synaptic maturation. This suggests that while transcriptional signatures of maturation persist post-transplantation, they are accompanied by robust stress responses likely reflecting adaptation to the transplantation process or the host retinal environment. Overall, these findings underscore the progression of photoreceptor maturation post-transplantation into the host retina.

Pathway analysis highlights oxidative and metabolic stress in PRPCs transplanted into normal canine retinas

To identify pathways contributing to increased cell death of transplanted PRPCs, we compared gene expression profiles between transplanted and in vitro cultured cells of each identified cell type. Differentially expressed genes were analyzed using Ingenuity Pathway Analysis (IPA) to identify enriched pathways specific to the transplanted cells. The top 30 enriched pathways identified through IPA, with Benjamini–Hochberg adjusted p-values < 0.05, are presented in Fig. 5a. Several pathways were consistently enriched across the different cell types.

Most notably, 20 of these pathways (Fig. 5b) indicate that the majority of transplanted cells experience significant oxidative and metabolic stress. The top differentially regulated pathways, including *Parkinson's Signaling Pathway*, *Mitochondrial Dysfunction*, and *Sirtuin Signaling Pathway*, are upregulated in all but one cell cluster. This widespread activation of stress-related pathways suggests that transplanted cells are mounting an adaptive metabolic response to the subretinal environment, engaging mechanisms linked to oxidative stress, mitochondrial maintenance, and cellular repair. In contrast, pathways essential for mitochondrial energy production, such as *Formation of ATP by Chemiosmotic Coupling*, *Cristae Formation*, *Complex IV Assembly*, *Complex I Biogenesis*, and *Oxidative Phosphorylation*, are markedly downregulated. Similarly, *TP53 Regulation of Metabolic Genes* and *Respiratory Electron Transport* pathways exhibit significant suppression, indicating compromised

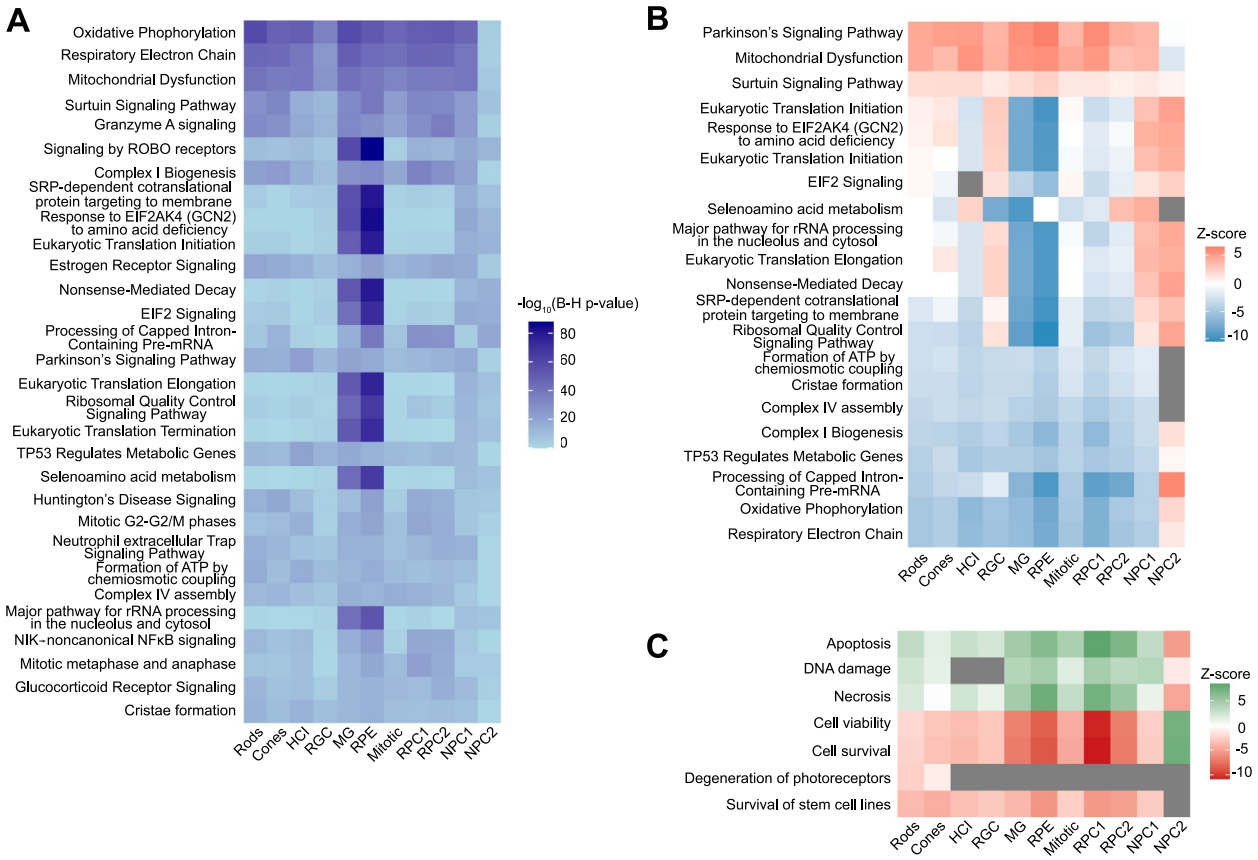

Fig. 5 Pathway analysis reveals key biological processes impacted in cultured vs. transplanted PRPCs. **a** Ingenuity Pathway Analysis (IPA) identifies the top 30 significantly differentially regulated pathways in transplanted PRPCs, with Benjamini–Hochberg (B–H) adjusted p-values ≤ 0.05. **b** Heatmap of activation z-scores for 20 of the top 30 pathways highlights substantial metabolic dysregulation and oxidative stress in transplanted PRPCs. Gray boxes represent pathways or functions where IPA could not reliably predict the activation state. **c** IPA disease and functions analysis indicates an upregulation of cell death-related pathways in transplanted PRPCs, visualized as a heatmap of differentially regulated functions.

metabolic activity and diminished mitochondrial function. The observed downregulation of these pathways reflects a reduction in cellular energy production and metabolic efficiency, likely driven by the transition from a nutrient-rich culture environment to that of the subretinal space. Furthermore, the downregulation of *Processing of Capped Intron-Containing Pre-mRNA* suggests disruptions in nuclear processing critical for cellular function.

Although oxidative and metabolic stress pathways were enriched across all donor cell types, Müller glia and RPE cells exhibited the most significant transcriptional shifts, both in terms of pathway enrichment p-values and magnitude of activation/inhibition z-scores. This likely reflects their specialized roles in sensing and responding to metabolic stress and may signal the early initiation of a support response to stabilize the transplant environment.

Disease and function analysis in IPA (Fig. 5c) further supports these findings, showing increased activation of apoptotic and necrotic cell death pathways alongside decreased cell viability and survival. These trends are consistent across all cell types except the NPC2 cluster, where upregulation of energy production pathways (Fig. 5b) and greater resilience to the subretinal environment were observed, likely reflecting different energy demands and enhanced adaptability of this cell population.

Overall, these results suggest that the significant early loss of transplanted PRPCs is driven by metabolic reprogramming in response to a change in nutrient availability in the subretinal environment. This shift, coupled with oxidative stress and impaired mitochondrial function, likely contributes to the high rates of cell death observed shortly after transplantation.

Host retinal responses to PRPC transplantation are associated with metabolic reprogramming, immune activation, and translational adaptation

To characterize the host retinal response to transplanted cells, we analyzed retinal cells from normal canine hosts by comparing differential gene expression in cells directly overlying the transplanted PRPCs with cells collected from regions devoid of transplanted cells. Using expression of established cell-type markers, we identified all major retinal cell types, including rods, cones, rod bipolar cells, ON cone bipolar cells, OFF cone bipolar cells, amacrine cells, horizontal cells, retinal ganglion cells, Müller glia, astrocytes, and microglia (Fig. 6a–b). Pathway analysis revealed distinct changes in cellular processes among many host cell clusters, which were categorized into five functional groups (Fig. 6c): mitochondrial function and energy metabolism, protein translation and processing, amino acid regulation and metabolism, immune response and inflammation, and RNA processing.

Within mitochondrial function and energy metabolism, *Oxidative Phosphorylation*, *Respiratory Electron Transport*, and *Complex I Biogenesis* were upregulated in host cells overlaying the transplanted PRPCs, suggesting an enhanced capacity for mitochondrial energy production. This is likely to reflect increased energy demands or compensatory mechanisms to counteract local stress. Paradoxically, *Mitochondrial Dysfunction* and *Sirtuin Signaling Pathways* were concurrently downregulated, which may indicate reduced activation of stress response and repair mechanisms essential for mitochondrial maintenance. This suggests that, despite an enhanced capacity for energy production, the ability to sustain mitochondrial health under stress may be compromised. Pathways related to protein translation and processing were broadly upregulated, including *Nonsense-Mediated Decay (NMD)*, *Eukaryotic Translation Initiation and Elongation*, and *Ribosomal Quality Control Signaling*. These findings point to increased demands for protein synthesis and quality control, likely reflecting cellular efforts to adapt to stress conditions. Similarly, pathways involved in metabolic adaptation, such as *Response of EIF2AK4 to Amino Acid Deficiency*, *EIF2 Signaling*, and *Selenoamino Acid Metabolism*, were upregulated, highlighting nutrient stress and the need for tight regulation of amino acid availability. Immune response and inflammatory pathways were prominently activated, as evidenced by the upregulation of *Neutrophil Degranulation* and *Neutrophil Extracellular Trap Signaling*. These findings underscore a robust local inflammatory response at the transplant-host interface, likely driven by the presence of transplanted cells and not adequately suppressed by immunosuppression treatment. Additionally, RNA processing pathways, including *Major Pathway of rRNA Processing* and *Processing of Capped Intron-Containing Pre-mRNA*, were upregulated, suggesting enhanced transcriptional and translational activity to maintain cellular homeostasis under stress. Finally, the downregulation of *Visual Phototransduction* suggests localized dysfunction or reduced phototransduction activity in photoreceptors adjacent to the transplanted cells.

Interestingly, no significant pathway changes were detected in horizontal cells or retinal ganglion cells, suggesting that these cell types are not actively involved in responding to the transplanted PRPCs. Collectively, these findings reveal a complex interplay of metabolic reprogramming, immune activation, and translational adaptation in host retinal cells directly in contact with the PRPCs. The simultaneous upregulation of mitochondrial energy production pathways and downregulation of mitochondrial maintenance pathways underscores the

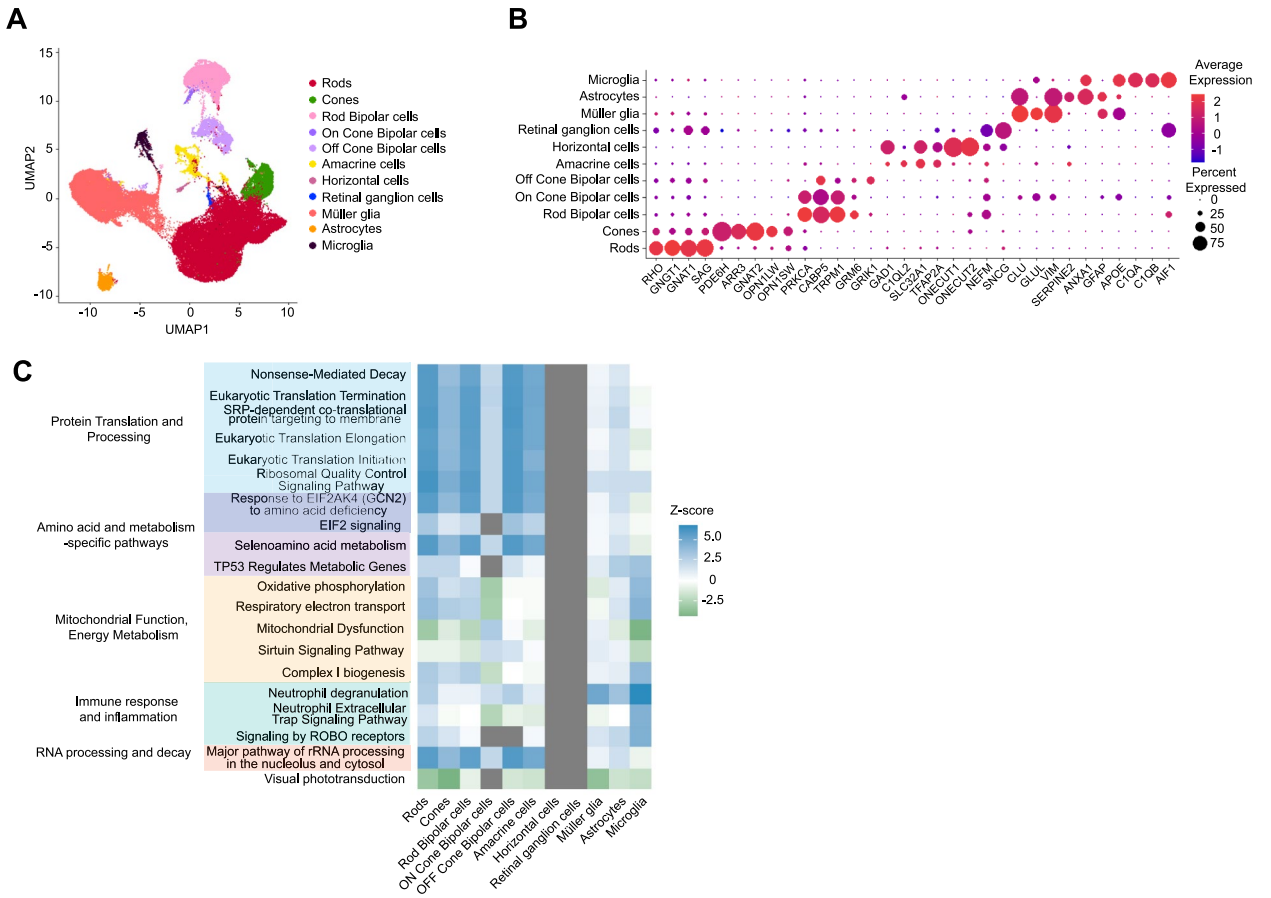

Fig. 6 Single-cell RNA sequencing analysis of canine host neuroretina overlying transplanted cells compared to non-transplanted areas. **a** UMAP plot illustrating distinct cell clusters identified in the canine neuroretina overlying the graft, with each cluster corresponding to a specific retinal cell type. Similar clusters were also identified from neuroretina outside the transplanted region (not shown). **b** Dot plot illustrating expression levels of key marker genes used to annotate retinal cell types within the clusters. **c** Heatmap of top differentially regulated pathways, with Benjamini-Hochberg (B-H) adjusted p-values ≤ 0.05 identified by IPA, grouped into distinct biological categories. Gray boxes represent pathways or functions where IPA was unable to reliably predict the activation state

metabolic strain at the transplant–host interface, while heightened inflammation and translational reprogramming reflect the cellular challenges of adapting to the altered microenvironment.

Immunohistochemical evidence confirms oxidative and cell stress responses in transplanted PRPCs and host photoreceptors

To validate the transcriptomic findings from both transplanted PRPCs and the adjacent host retinal cells, we examined oxidative stress, mitochondrial integrity, and cell death markers using immunohistochemistry. This analysis enabled direct visualization of stress-related phenotypes and allowed us to determine whether the transcriptional changes observed in scRNAseq data were reflected at the protein level in situ. We stained for 4-hydroxynonenal (4-HNE, a marker of oxidative lipid peroxidation), ATP5A (ATP synthase F1 subunit alpha; a mitochondrial marker), cleaved caspase-3 (apoptosis marker), and HMGB1 (High Mobility Group Box 1, a nuclear protein that translocates to the cytoplasm during necrotic or inflammatory stress). For comparison, dissociated PRPCs from retinal organoids (ROs) were cultured in vitro for 3 days and processed similarly.

4-Hydroxynonenal staining was prominent in the host outer nuclear layer (ONL), particularly in photoreceptor inner segments and cell bodies, indicating oxidative stress in host photoreceptors overlying the transplanted PRPCs (Fig. 7A1). Transplanted PRPCs in the subretinal space also exhibited 4-HNE staining, though the signal was less intense and more variable (Fig. 7A2). In contrast, cultured PRPCs showed minimal 4-HNE signal (Fig. 7A3), suggesting that oxidative stress observed in vivo is driven by the host environment. Staining for ATP5A revealed strong and uniform mitochondrial expression in the host ONL (Fig. 7B1), consistent with intact mitochondrial

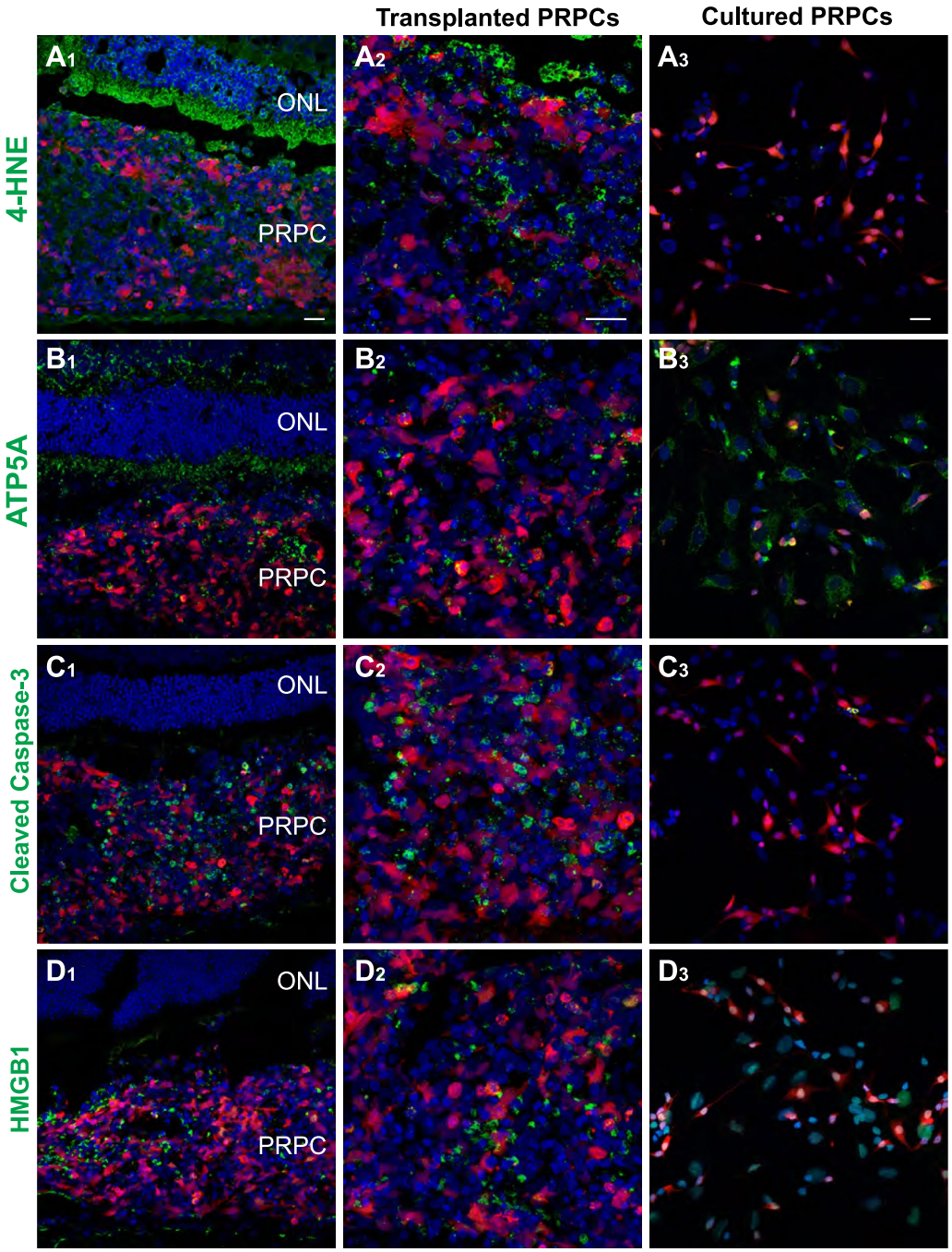

Fig. 7 Immunohistochemical evidence of oxidative stress, mitochondrial dysfunction, and cell death in transplanted PRPCs. **A_1–A_3** 4-Hydroxynonenal (4-HNE) staining with (**A_1–A_2**) showing transplanted cells at 3 days post-injection and **A_3** showing cultured dissociated PRPCs. **B_1–B_3** ATP5A staining in transplanted PRPCs **(B_1–B_2)** compared to cultured controls **(B_3). C_1–C_3** Cleaved caspase-3 staining apoptotic PRPCs in vivo **C_1–C_2** versus absence of signal in cultured PRPCs **(C_3). D_1–D_3** Cytoplasmic HMGB1 staining in transplanted cells **(D_1–D_2)**, consistent with necrotic or stressed states, while remaining nuclear in cultured PRPCs (**D_3**). Scale bar = 20 µms

structure and sustained energy production capacity in host photoreceptors. In contrast, ATP5A staining in the adjacent transplanted PRPCs (Fig. 7B2) appeared weaker and more heterogeneous, indicating early mitochondrial compromise. Cultured PRPCs displayed robust and uniform ATP5A staining (Fig. 7B3), similar to the host ONL, reflecting healthy mitochondrial function under in vitro conditions.

Cleaved caspase-3 staining (Fig. 7C1–2) revealed apoptosis in a subset of transplanted PRPCs, consistent with the IPA-predicted activation of apoptotic pathways. In contrast, neither host photoreceptors nor cultured PRPCs showed appreciable cleaved caspase-3 signal (Fig. 7C3), indicating that cell death at this early time point is largely restricted to donor cells. Similarly, HMGB1 exhibited cytoplasmic localization in transplanted PRPCs (Figs. 7D1–2), indicative of necrotic or inflammatory stress. Cultured PRPCs retained nuclear HMGB1 localization (Fig. 7D3), further confirming the in vivo specificity of the stress response.

Together, these findings confirm that the subretinal environment induces early oxidative damage, mitochondrial dysfunction, and activation of both apoptotic and necrotic stress pathways in transplanted PRPCs. In contrast, host photoreceptors also exhibit oxidative stress but appear to avoid widespread cell death, suggesting that they may be better equipped to manage the metabolic and environmental stress induced by transplantation. These protein-level observations validate and reinforce the transcriptomic findings from both donor and host cell populations, underscoring the biological significance of early stress responses at the transplant interface.

Microglial infiltration and activation following PRPC transplantation into normal retina are primarily directed towards clearing apoptotic PRPCs

Microglia, the primary resident immune cells of the retina, demonstrated active infiltration into the outer retina and migration towards the PRPCs (Fig. 8A1–2). In contrast, microglia remained confined to the inner retinal space in regions devoid of PRPCs (Fig. 8B). Figure 8C1–3 show high magnification images of Iba1-positive microglia closely associated with tdTomato-positive PRPCs in the subretinal space. Several of these donor cells exhibit pyknotic nuclei (yellow arrows) indicative of apoptosis or necrosis. The spatial proximity and morphology suggest that microglia are actively engaging and engulfing dying PRPCs.

To further investigate the role of microglia and other glial cells, such as astrocytes and Müller glia, in the host response, we analyzed pathways specifically upregulated in these cell populations. These pathways spanned five functional categories: immune response and inflammation, autophagy and cellular regulation, cell morphology and cytoskeletal dynamics, DNA synthesis and replication, and cell cycle and proliferation (Fig. 8d).

Immune response pathways, including *Neutrophil Degranulation*, *Class I MHC-Mediated Antigen Processing and Presentation*, and *C-Type Lectin Receptors* (CLRs), were significantly upregulated, indicating an active immune response likely driven by the recognition of transplanted cells as foreign or stressed. Additionally, the upregulation of the *TNFR2 Non-Canonical NF-κB Pathway*, *NIK–>Noncanonical NF-κB Signaling*, and *T and B Cell Receptor Signaling pathways* further suggests the engagement of both innate and adaptive immune mechanisms. These findings point to a coordinated immune activation within the retinal microenvironment, likely involving both resident immune cells and cellular signaling pathways typically associated with adaptive immunity, even in the absence of direct T and B cell infiltration.

Pathways related to cellular regulation and stress adaptation, such as *Microautophagy Signaling* and *PTEN Regulation*, were also upregulated, suggesting that glial cells were mobilizing regulatory mechanisms to maintain homeostasis in response to the transplantation-associated stress. Concurrently, upregulation of cytoskeletal and adhesion pathways, including *Actin Cytoskeleton Signaling*, *RHOA Signaling*, *Integrin Signaling*, and *Signaling by Rho Family GTPases*, indicated extensive cellular remodeling. These changes likely facilitate interactions with transplanted cells and contribute to reshaping the host microenvironment. Notably, upregulation of pathways involved in proliferation and DNA synthesis, such as *Synthesis of DNA*, *DNA Replication Pre-Initiation*, and mitotic phase-related pathways (*Mitotic G2-G2/M Phases* and *Regulation of Mitotic Cell Cycle*), suggests a robust gliotic response characterized by increased glial proliferation, potentially aimed at repairing or remodeling retinal architecture in the transplant region.

Together, these findings underscore a multifaceted host response to the transplanted PRPCs. The response is characterized by microglial activation, immune signaling, cytoskeletal remodeling, and glial proliferation, reflecting

(See figure on next page.)

Fig. 8 Microglial response to donor human PRPCs in normal canine retinas 3 days post-xenotransplantation. Immunohistochemical analysis of microglial activation and migration in normal dogs (n = 2). Image shown is from dog LG5. **A_{1-2}** Host Iba1-positive microglia migrated into the host subretinal space and infiltrated the Td-tomato-positive donor PRPC mass. **B** In retinal regions distant from the transplantation site, microglia remain restricted to their native locations within the inner retina. **C_{1-3}** Higher magnification images showing Iba1-positive microglia apposed to tdTomato-positive donor cells with pyknotic nuclei (yellow arrows). **D** Ingenuity Pathway Analysis (IPA) of top enriched pathways in microglial, Müller glial, and astrocytic populations isolated from host retinas 3 days post-transplantation. Scale bar = 20 µms

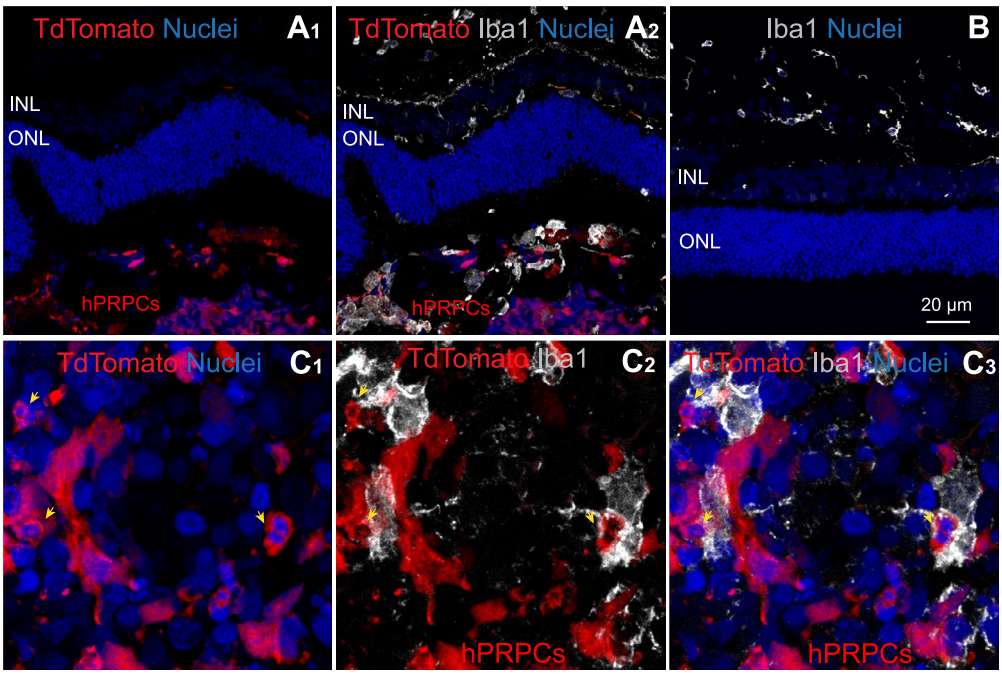

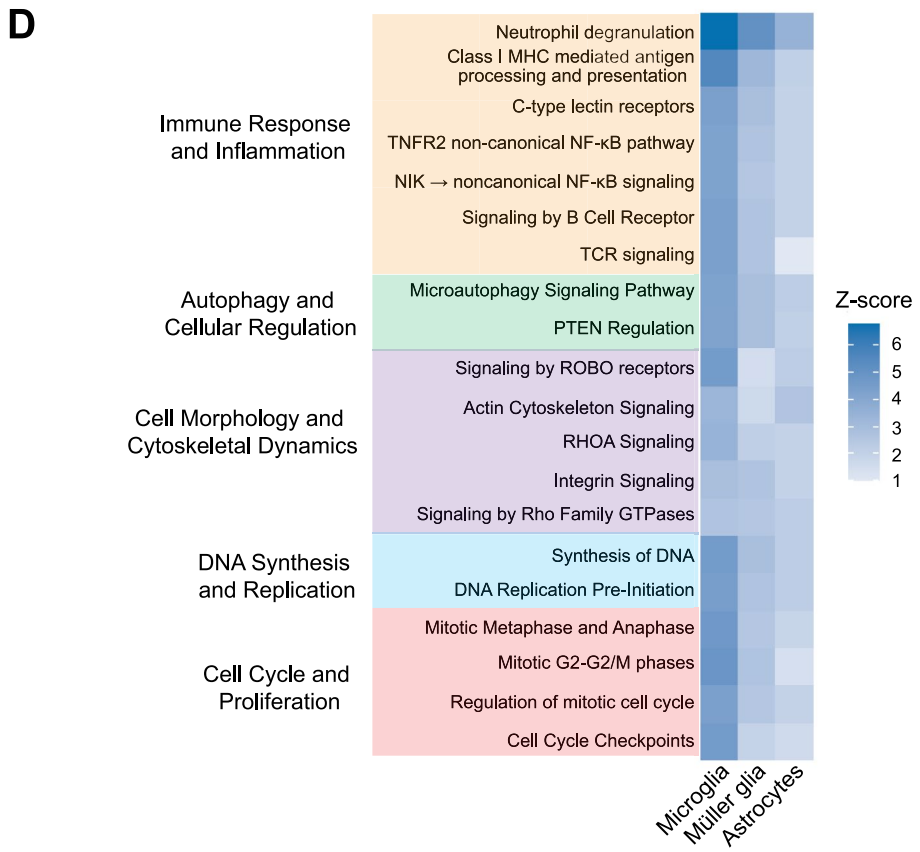

Fig. 8 (See legend on previous page.)

a coordinated effort to manage transplantation-induced stress and integrate the transplanted cells into the host retina. However, these processes also highlight potential challenges to graft survival and successful integration due to the complexity of the immune and cellular dynamics at the host-transplant interface.

Discussion

The findings from this study offer crucial insights into the challenges associated with PRPC xenotransplantation into the subretinal space. Despite the potential of PRPCs to restore vision in animal models with retinal degenerative diseases [4–6], significant early cell loss observed after transplantation remains a barrier to long-term graft survival and functional recovery. Consistent with previous reports [2, 13, 14], our study demonstrated substantial loss of transplanted cells within the first week after subretinal injection. This was observed despite immunosuppression across different retinal conditions, spanning from healthy normal retinas to mutant retinas with end stage degeneration. While retinal degeneration introduces additional challenges to cell survival, the early loss of PRPCs appears to be a distinct phenomenon, driven by mechanisms that are independent of the degenerative status of the retina.

Early cell loss in transplanted PRPCs is due to metabolic stress

The substantial early loss of grafted cells is not unique to PRPC transplantation. Similar observations have been reported in studies of neuronal progenitor cell transplantation into the central nervous system, where significant cell death occurs within the first seven days post-transplantation [32–35]. This suggests that early cell loss may be a general phenomenon associated with cell transplantation, irrespective of the target tissue.

Our observations suggest that the early loss of PRPCs is primarily due to metabolic stress as the cells transition from a nutrient-rich culture environment to the relatively nutrient-poor subretinal space. In native retina, photoreceptors thrive within a specialized metabolic relationship with the retinal pigment epithelium (RPE) and Müller glia, which support their high energy demands [36, 37]. Transplanted PRPCs, however, are not immediately integrated into this metabolic network, leaving them vulnerable to stress-induced cell death. Transcriptomic analysis revealed that upon transplantation into subretinal space, PRPCs undergo substantial metabolic reprogramming; critical mitochondrial pathways, including oxidative phosphorylation and ATP production, are downregulated with concurrent upregulation of stress responsive pathways such as mitochondrial dysfunction and sirtuin signaling pathways. These findings were further supported by protein-level evidence of oxidative stress, mitochondrial compromise, and activation of apoptotic and necrotic pathways, underscoring the multifaceted cellular stress encountered by transplanted cells in vivo. Although we cannot rule out the possibility that systemic immunosuppressive drugs contribute to the observed stress responses in transplanted donor cells, these effects cannot be disentangled in the current model, and future studies comparing alternative immunosuppression protocols will be necessary to address this limitation. Additionally, to minimize confounding effects from host retinal degeneration - such as gliosis, structural disorganization, and inflammation - we performed single-cell RNA sequencing in wild-type animals. While this allowed us to isolate donor cell-intrinsic responses to the subretinal environment, it does not capture the influence of a degenerating host retina on donor cell fate. Future studies will be needed to assess how degeneration-associated changes in the host microenvironment alter stress responses, survival, and integration outcomes.

While metabolic stress likely drives early cell death, but RNA velocity analysis provides additional insights into the fate and maturation of the surviving PRPCs in the host environment. This analysis highlights the dynamic transcriptional trajectories of transplanted cells, revealing that the subretinal space can support further photoreceptor maturation. For cones, RNA velocity vectors indicate progression toward transcriptional states associated with mature cones, suggesting that the host retinal environment provides cues to promote their differentiation. In contrast, cone cells maintained in culture conditions retained transcriptional profiles consistent with immaturity, highlighting the importance of the in vivo environment for maturation. It is important to note that RNA velocity reflects inferred transcriptional dynamics and not definitive evidence of morphological or functional maturation. These results suggest that the subretinal environment is permissive of ongoing photoreceptor development. Similarly, rods exhibited continued maturation under both conditions, but the host retina better supported the advanced maturation of the most developed rods. These findings suggest that although the subretinal space presents metabolic challenges leading to substantial cell loss, it also provides essential signals that facilitate the progression of surviving cells toward mature photoreceptor states. This observation aligns with previous long-term studies in murine models [38], which similarly demonstrated enhanced photoreceptor maturation in the subretinal space, and with our own findings from long-term studies in immunosuppressed normal dogs [2]. Together, these results suggest that the subretinal environment provides evolutionarily conserved cues that support photoreceptor development across species and

disease context. This consistency across models underscores the robustness of subretinal cues in promoting photoreceptor lineage progression. Notably, our morphological observations (Fig. 3) and RNA velocity analyses raise the possibility that subretinal environment may preferentially support cone photoreceptor maturation or survival. However, future studies using matched long-term in vitro and in vivo samples from the same donor RO batches will be critical to distinguish between differential maturation, survival, and lineage commitment outcomes.

This interplay between early metabolic challenges and the host environment's supportive cues underscores the need for strategies that mitigate stress while enhancing cell survival and integration. Targeting metabolic pathways or preconditioning PRPCs to endure nutrient deprivation and oxidative stress prior to transplantation represents a promising avenue [39, 40]. Strategies such as transplanting PRPCs in either hydrogels [41, 42] or biodegradable scaffolds [43, 44] that would also allow the slow release of nutrients, or alternatively, gradually adapting cells to a low nutrient environment before transplantation, could potentially mitigate early cell loss and improve graft survival.

Finally, while our analysis emphasizes metabolic stress as a primary early challenge for transplanted PRPCs, we also identified significant enrichment of other cellular stress pathways. Notably, our IPA results revealed activation of ER stress-related signaling (e.g., EIF2 Signaling), apoptosis-related pathways (e.g., TP53-Regulated Metabolic Genes, Granzyme A Signaling), and immune-associated signaling (e.g., NIK → Noncanonical NF-κB Signaling). These findings suggest that, in addition to mitochondrial dysfunction and oxidative stress, transplanted cells experience a broader range of stress responses during early adaptation. Many of these non-metabolic pathways may represent downstream consequences of the initial metabolic insult, reflecting the interconnected nature of stress response networks. Nevertheless, we acknowledge that analyzing only a single early time point limits our ability to capture the full trajectory of cell fate decisions. Future studies incorporating later post-transplantation time points will be critical to better understand how these early stress responses evolve and contribute to longer-term survival or degeneration.

Retinal environment in end stage degeneration is not conducive to long-term PRPC survival

While early cell death after transplantation is primarily driven by metabolic stress and potentially also by cell damage resulting from the surgical procedure, the continued loss of PRPCs in end-stage degenerative retinas point to additional challenges distinct from those in the early phase. The extent of retinal degeneration, particularly the structural integrity of the host ONL, appears to play a critical role in determining graft survival and integration outcomes. A recent study in the cpfl1 mouse model of cone degeneration, where the ONL remains near normal due to the preservation of rods, showed improved PRPC integration, polarization and differentiation compared to transplantation in mice with end stage retinal degeneration [4]. Similarly, in this study, the survival and integration of PRPCs differed significantly between mutant canine models with varying degrees of ONL preservation. Disruption of the external limiting membrane (ELM), commonly observed in degenerated retinas, may facilitate donor cell entry into the ONL. In such regions, donor cells likely integrate through lateral displacement of remaining host photoreceptors rather than active replacement. In retinas with three or more rows of photoreceptor nuclei (late-stage degeneration), PRPCs were more likely to establish connections with host cells, benefiting from the residual retinal architecture that supports integration and radial polarization. Structural support from neighboring host photoreceptors and Müller cells, along with molecular cues, likely contributed to the differentiation of the PRPCs into elongated cells that adopt a photoreceptor-like morphology with the formation of an inner segment, a short outer segment, an axon, and a pedicle-like synaptic terminal. While these structural features suggest potential for synaptic maturation, future studies will need to evaluate synaptic integration more comprehensively using additional synaptic markers (e.g., ribeye, PSD95), ultrastructural tools such as Ultrastructure Expansion Microscopy (UExM), and functional assays including multielectrode array recordings or cortical fMRI to determine whether donor-host connections are functionally active.

In contrast, retinas with a single row of nuclei (end-stage degeneration) presented a harsher microenvironment characterized by disrupted extracellular matrix signals and reduced structural and trophic support. These factors likely impede PRPC differentiation into more normal photoreceptors, increase their susceptibility to stress and apoptosis, and contribute to continued loss of transplanted cells. The use of biocompatible biodegradable 3D scaffolds to locally deliver a high density of PRPCs and promoting their polarization [43–45] may address these challenges and expand the therapeutic window of PRPC transplantation to end-stage disease.

The role of the host immune response in exacerbating transplanted cell loss remains complex. As demonstrated in our previous study using the rcd1/*PDE6B* model at late stages of degeneration, host innate immune cells (Iba1- and CD18-positive) infiltrated the transplanted cell mass [2]. However, with the continued immunosuppressive

treatment, the transplanted cells survived long term in the host ONL and INL. Similarly, in the current study with the xlpra2/*RPGR* model at a comparable late stage of degeneration, immunosuppression proved effective in promoting PRPC survival. These findings suggest that while immune cell infiltration occurs, immunosuppression can mitigate its impact on transplanted cell survival, provided that the host retina retains some structural integrity (ONL thickness ≥ 3 rows of nuclei) and adequate trophic support is available.

We acknowledge that some of the key findings in this study, particularly those related to long-term donor cell survival and integration in late-stage degeneration, are based on a single xlpra2/*RPGR* dog followed for 22 weeks. While this represents a limitation, we believe the detailed characterization of this case provides important proof-of-concept data. These observations are supported by similar trends in our rcd1/*PDE6B* model (late-stage degeneration with ~ 2 ONL rows) [2], and are contrasted by the poor donor cell survival seen in the four $RHO^{T4R/+}$ dogs and the 88-week-old xlpra2/*RPGR* dog, both representing end-stage degeneration. Together, these findings strengthen the hypothesis that ONL preservation is a critical determinant of graft success. We recognize the need for larger cohorts to validate and expand upon these results, but we present this case to help inform the design of future studies by highlighting key variables, such as disease stage, ONL architecture, and early graft survival, that may influence transplant outcomes.

The host retina undergoes metabolic stress and activates a microglial response to transplanted cells

Host retinal cells overlying the transplanted PRPCs exhibited a complex interplay of metabolic, inflammatory, and translational changes. The upregulation of mitochondrial energy production pathways in host cells likely reflects a compensatory mechanism to meet increased energy demands or to support local stress responses. However, simultaneous downregulation of mitochondrial maintenance pathways indicates that this adaptation may come at the cost of long-term cellular health. The robust activation of immune and inflammatory pathways, including neutrophil degranulation and neutrophil extracellular trap signaling, highlights the host's response to transplanted cells as a significant contributor to the transplant's microenvironment. Microglial infiltration and activation further underscore the immune system's involvement in shaping the transplant's fate. In our earlier study [2], we observed that PRPCs transplanted into the subretinal space of normal, immunosuppressed dogs did not elicit microglial migration when examined at a late time point - 12 weeks post-transplantation. The grafts remained confined to the subretinal region, with no microglial infiltration into the graft cell mass or the ONL. In contrast, in the current study focused on the early post-transplant period, we observed microglial infiltration into the graft site as early as 3 days after transplantation. Given the cell death observed in transplanted PRPCs, it is likely that microglial activation initially serves a phagocytic role, clearing apoptotic and necrotic cells rather than mounting an immune response against the graft itself. Nonetheless, we cannot exclude the possibility that activated microglia may also contribute to further cell loss through the release of pro-inflammatory cytokines or neurotoxic factors. Pharmacologic modulation of microglial activation - such as with minocycline, which has been shown to suppress microglial-driven inflammation in retinal and CNS injury models [46, 47] - may help distinguish whether early microglial responses are protective, phagocytic, or harmful. Such interventions could clarify the functional role of microglia in this context and guide future strategies to enhance transplant success. While our immunosuppression regimen appears effective in limiting adaptive immune responses [2], these findings indicate that innate immune activation still occurs in the early post-transplant period. Even in the absence of classical immune rejection, this innate response may significantly influence the early graft microenvironment. These observations highlight the need for future strategies aimed at modulating local innate immune responses in combination with approaches that enhance donor cell survival, reduce metabolic stress, and promote adaptive cellular reprogramming.

Conclusions

The results of this study provide valuable insights into the multifaceted challenges associated with PRPC transplantation in the context of retinal degenerative diseases. Cell loss, driven by metabolic stress-induced apoptosis and loss of structural and trophic support underscores the critical need for strategies that enhance the resilience of PRPCs in the subretinal space. Metabolic preconditioning, gradual adaptation to low-nutrient conditions prior to transplantation, and optimization of biomaterial carriers such as hydrogels or scaffolds, could serve as promising approaches to address these limitations. This study also points to the necessity of implementing photoreceptor replacement strategies that are tailored to the degree of retinal degeneration. Addressing both graft-intrinsic and host-environmental factors is essential to maximize the therapeutic potential of PRPC transplantation in treating retinal degenerative diseases.

While this study offers important insights, we acknowledge the limitation of using a xenotransplantation model. Immune responses in this context may not fully mirror

those seen in allograft settings relevant to clinical application. Moreover, our transcriptomic analyses were conducted in structurally intact, non-degenerating retinas, which differ significantly from the advanced degenerative states present in most patients. In advanced retinal degeneration, structural disorganization, gliosis, and impaired metabolic support may fundamentally alter the graft–host interface. Despite these differences, our findings suggest that a key determinant of graft success is the preservation of outer nuclear layer (ONL) structure. Based on this, we propose that the optimal clinical intervention window may lie in advanced - but not end-stage - disease, when there is still significant ONL retention to support donor cell integration. In this context, the metabolic stress observed in transplanted PRPCs is likely to remain a critical challenge, though its severity and downstream effects may vary with disease stage. Additionally, although this study used ESC-derived PRPCs, future therapeutic applications will rely on donor iPSC-derived cells. Donor heterogeneity may influence transplant outcomes and remains an important area for future investigation. Collectively, these results emphasize the importance of pairing cell-intrinsic strategies that improve donor cell resilience with host-targeted approaches that preserve retinal architecture and mitigate environmental stress. Future studies in models that more accurately reflect the clinical disease state will be essential for refining timing, optimizing delivery, and ultimately translating photoreceptor replacement into durable therapeutic benefit. With continued progress, PRPC transplantation holds strong promise as a broadly applicable therapeutic approach for patients with inherited retinal degenerations.

Abbreviations

PRPC	Photoreceptor precursor cell
scRNAseq	Single-cell RNA sequencing
ESC	Embryonic stem cell
cSLO	Confocal scanning laser ophthalmoscopy
OCT	Optical coherence tomography
ONL	Outer nuclear layer
PI	Post-injection

Supplementary Information

The online version contains supplementary material available at https://doi.org/10.1186/s13287-025-04509-w.

Additional file1 (PDF 1529 KB)

Acknowledgements
We express our gratitude to the staff of the Retinal Disease Studies Facility at the University of Pennsylvania for their outstanding animal care, and to Ms. Lydia Melnyk (senior research coordinator). The authors declare that they have not use AI-generated work in this manuscript.

Author contributions
Conceptualization: R.S., W.A.B., D.M.G.; Methodology: R.S., N.D., A.L.M., J.K., E.K., P.B., W.A.B.; Software: R.S., E.K., P.B.; Validation: R.S.; Formal analysis: R.S., J.K. A.G., Y. S., E.K., P.B., W.A.B.; Investigation: R.S., N.D., J.K., A.G., Y.S., E.K., P.B., W.A.B.; Resources: D.M.G., G.D.A., W.A.B.; Data Curation: R.S.; Writing-Original Draft: R.S., W.A.B.; Writing-Review and Editing: all authors; Visualization: R.S., E.K., P.B., W.A.B.; Supervision: W.A.B.; Project administration: R.S., W.A.B., Funding acquisition: R.S., D.M.G., J.H.W., G.D.A, W.A.B.

Funding
This study was supported by; NIH/NEI grants U24EY029890, RO1EY006855, and P30EY001583, Fighting Blindness Canada Vision 20/20 grant, The Foundation Fighting Blindness, The Van Sloun Fund for Canine Genetic Research, Research to Prevent Blindness, the Sandra Lemke Trout Chair in Eye Research, and the Retina Research Foundation Emmett A. Humble Distinguished Directorship of the McPherson Eye Research Institute (DMG).

Availability of data and materials
Single-cell RNA-sequencing data, including raw files and processed matrices, have been deposited in the GEO database under accession numbers: GSE285393 and GSE285735. The code used for data analysis is available upon request from R.S. and P.B.

Declarations

Ethics approval and consent to participate
All procedures involving dogs adhered to the ARVO Statement for the Use of Animals in Ophthalmic and Vision Research and were approved by the Institutional Animal Care and Use Committee (IACUC) at the University of Pennsylvania (Protocol #803254, titled *Gene, Medical, and Cell Therapies for Canine Retinal Degenerative Diseases*, approved on October 9, 2022).

Human or animal participants
All experiments involving human embryonic stem cell (hESC) line (WA09 cells purchased from WiCell) were performed in accordance with relevant guidelines and regulations of the NIH (NIH Approval Number: NIHhESC-10–0062) and the provider (WiCell). The WA09 cell line is listed on the NIH Human Embryonic Stem Cell Registry and was derived with documented donor informed consent and institutional ethical approval, as required for NIH registration.

Consent for publication
All authors confirm their consent for publication.

Competing interests
D.M.G. is an inventor on patents related to generation of 3D ROs (US PTO no. 9,328,328) filed by the Wisconsin Alumni Research Foundation (Madison, WI, USA). D.M.G. has ownership interest in and receives grant funding from Opsis Therapeutics, LLC, which has licensed the technology to generate 3D ROs. The terms of this arrangement have been reviewed and approved by the University of Wisconsin-Madison in accordance with its conflict- of-interest policies. D.M.G. (Opsis Therapeutics, LLC) holds US Patent No. US9752119B2 (OV patent). All other authors declare no conflicts of interest.

Author details
[1]Division of Experimental Retinal Therapies, Department of Clinical Sciences & Advanced Medicine, School of Veterinary Medicine, University of Pennsylvania, Philadelphia, PA 19104, USA. [2]Waisman Center, University of Wisconsin-Madison, Madison, WI 53705, USA. [3]Schepens Eye Research Institute of Massachusetts Eye and Ear, Boston, MA 02114, USA. [4]Department of Ophthalmology, Harvard Medical School, Boston, MA 02114, USA. [5]Walter Flato Goodman Center for Comparative Medical Genetics, School of Veterinary Medicine, University of Pennsylvania, Philadelphia, PA 1904, USA. [6]Children's Hospital of Philadelphia, Philadelphia, PA 19104, USA. [7]McPherson Eye Research Institute, University of Wisconsin-Madison, Madison, WI 53705, USA. [8]Department of Ophthalmology and Visual Sciences, University of Wisconsin-Madison, Madison, WI 53705, USA.

Received: 21 February 2025 Accepted: 3 July 2025
Published online: 25 July 2025

References

1. Hambright D, Park KY, Brooks M, McKay R, Swaroop A, Nasonkin IO. Long-term survival and differentiation of retinal neurons derived from human embryonic stem cell lines in un-immunosuppressed mouse retina. Mol Vis. 2012;18:920–36.
2. Ripolles-Garcia A, Dolgova N, Phillips MJ, Savina S, Ludwig AL, Stuedemann SA, et al. Systemic immunosuppression promotes survival and integration of subretinally implanted human ESC-derived photoreceptor precursors in dogs. Stem Cell Reports. 2022;17(8):1824–41.
3. Tu HY, Watanabe T, Shirai H, Yamasaki S, Kinoshita M, Matsushita K, et al. Medium- to long-term survival and functional examination of human iPSC-derived retinas in rat and primate models of retinal degeneration. EBioMedicine. 2019;39:562–74.
4. Gasparini SJ, Tessmer K, Reh M, Wieneke S, Carido M, Volkner M, et al. Transplanted human cones incorporate into the retina and function in a murine cone degeneration model. J Clin Invest. 2022;132(12).
5. Ribeiro J, Procyk CA, West EL, O'Hara-Wright M, Martins MF, Khorasani MM, et al. Restoration of visual function in advanced disease after transplantation of purified human pluripotent stem cell-derived cone photoreceptors. Cell Rep. 2021;35(3): 109022.
6. McLelland BT, Lin B, Mathur A, Aramant RB, Thomas BB, Nistor G, et al. Transplanted hESC-derived retina organoid sheets differentiate, integrate, and improve visual function in retinal degenerate rats. Invest Ophthalmol Vis Sci. 2018;59(6):2586–603.
7. Yamasaki S, Sugita S, Horiuchi M, Masuda T, Fujii S, Makabe K, et al. Low immunogenicity and immunosuppressive properties of human ESC- and iPSC-derived retinas. Stem Cell Reports. 2021;16(4):851–67.
8. Streilein JW. Ocular immune privilege: the eye takes a dim but practical view of immunity and inflammation. J Leukoc Biol. 2003;74(2):179–85.
9. Zamiri P, Sugita S, Streilein JW. Immunosuppressive properties of the pigmented epithelial cells and the subretinal space. Chem Immunol Allergy. 2007;92:86–93.
10. Keino H, Horie S, Sugita S. Immune privilege and eye-derived T-regulatory cells. J Immunol Res. 2018;2018:1679197.
11. Zhu J, Cifuentes H, Reynolds J, Lamba DA. Immunosuppression via loss of IL2rgamma enhances long-term functional integration of hESC-derived photoreceptors in the mouse retina. Cell Stem Cell. 2017;20(3):374-84e5.
12. Wenkel H, Streilein JW. Analysis of immune deviation elicited by antigens injected into the subretinal space. Invest Ophthalmol Vis Sci. 1998;39(10):1823–34.
13. West EL, Gonzalez-Cordero A, Hippert C, Osakada F, Martinez-Barbera JP, Pearson RA, et al. Defining the integration capacity of embryonic stem cell-derived photoreceptor precursors. Stem Cells. 2012;30(7):1424–35.
14. West EL, Pearson RA, Barker SE, Luhmann UF, Maclaren RE, Barber AC, et al. Long-term survival of photoreceptors transplanted into the adult murine neural retina requires immune modulation. Stem Cells. 2010;28(11):1997–2007.
15. Kennelly KP, Holmes TM, Wallace DM, O'Farrelly C, Keegan DJ. Early subretinal allograft rejection is characterized by innate immune activity. Cell Transplant. 2017;26(6):983–1000.
16. Jager LD, Canda CM, Hall CA, Heilingoetter CL, Huynh J, Kwok SS, et al. Effect of enzymatic and mechanical methods of dissociation on neural progenitor cells derived from induced pluripotent stem cells. Adv Med Sci. 2016;61(1):78–84.
17. Lowe A, Harris R, Bhansali P, Cvekl A, Liu W. Intercellular adhesion-dependent cell survival and rock-regulated actomyosin-driven forces mediate self-formation of a retinal organoid. Stem Cell Reports. 2016;6(5):743–56.
18. Seiler MJ, Aramant RB. Cell replacement and visual restoration by retinal sheet transplants. Prog Retin Eye Res. 2012;31(6):661–87.
19. Capowski EE, Samimi K, Mayerl SJ, Phillips MJ, Pinilla I, Howden SE, et al. Reproducibility and staging of 3D human retinal organoids across multiple pluripotent stem cell lines. Development. 2019;146(1).
20. Phillips MJ, Capowski EE, Petersen A, Jansen AD, Barlow K, Edwards KL, et al. Generation of a rod-specific NRL reporter line in human pluripotent stem cells. Sci Rep. 2018;8(1):2370.
21. Phillips MJ, Jiang P, Howden S, Barney P, Min J, York NW, et al. A novel approach to single cell RNA-sequence analysis facilitates in silico gene reporting of human pluripotent stem cell-derived retinal cell types. Stem Cells. 2018;36(3):313–24.
22. Thomson JA, Itskovitz-Eldor J, Shapiro SS, Waknitz MA, Swiergiel JJ, Marshall VS, et al. Embryonic stem cell lines derived from human blastocysts. Science. 1998;282(5391):1145–7.
23. Beltran WA, Hammond P, Acland GM, Aguirre GD. A frameshift mutation in RPGR exon ORF15 causes photoreceptor degeneration and inner retina remodeling in a model of X-linked retinitis pigmentosa. Invest Ophthalmol Vis Sci. 2006;47(4):1669–81.
24. Iwabe S, Ying GS, Aguirre GD, Beltran WA. Assessment of visual function and retinal structure following acute light exposure in the light sensitive T4R rhodopsin mutant dog. Exp Eye Res. 2016;146:341–53.
25. Sudharsan R, Simone KM, Anderson NP, Aguirre GD, Beltran WA. Acute and protracted cell death in light-induced retinal degeneration in the canine model of rhodopsin autosomal dominant retinitis pigmentosa. Invest Ophthalmol Vis Sci. 2017;58(1):270–81.
26. Satija R, Farrell JA, Gennert D, Schier AF, Regev A. Spatial reconstruction of single-cell gene expression data. Nat Biotechnol. 2015;33(5):495–502.
27. Stuart T, Butler A, Hoffman P, Hafemeister C, Papalexi E, Mauck WM 3rd, et al. Comprehensive integration of single-cell data. Cell. 2019;177(7):1888-902e21.
28. Danecek P, Bonfield JK, Liddle J, Marshall J, Ohan V, Pollard MO, et al. Twelve years of SAMtools and BCFtools. Gigascience. 2021;10(2).
29. La Manno G, Soldatov R, Zeisel A, Braun E, Hochgerner H, Petukhov V, et al. RNA velocity of single cells. Nature. 2018;560(7719):494–8.
30. Schindelin J, Arganda-Carreras I, Frise E, Kaynig V, Longair M, Pietzsch T, et al. Fiji: an open-source platform for biological-image analysis. Nat Methods. 2012;9(7):676–82.
31. Jacomy M, Venturini T, Heymann S, Bastian M. ForceAtlas2, a continuous graph layout algorithm for handy network visualization designed for the Gephi software. PLoS ONE. 2014;9(6): e98679.
32. Bacigaluppi M, Pluchino S, Peruzzotti-Jametti L, Kilic E, Kilic U, Salani G, et al. Delayed post-ischaemic neuroprotection following systemic neural stem cell transplantation involves multiple mechanisms. Brain. 2009;132(Pt 8):2239–51.
33. Hermann DM, Peruzzotti-Jametti L, Schlechter J, Bernstock JD, Doeppner TR, Pluchino S. Neural precursor cells in the ischemic brain - integration, cellular crosstalk, and consequences for stroke recovery. Front Cell Neurosci. 2014;8:291.
34. Korshunova I, Rhein S, Garcia-Gonzalez D, Stolting I, Pfisterer U, Barta A, et al. Genetic modification increases the survival and the neuroregenerative properties of transplanted neural stem cells. JCI Insight. 2020;5(4).
35. Li JY, Christophersen NS, Hall V, Soulet D, Brundin P. Critical issues of clinical human embryonic stem cell therapy for brain repair. Trends Neurosci. 2008;31(3):146–53.
36. Hurley JB. Retina metabolism and metabolism in the pigmented epithelium: a busy intersection. Annu Rev Vis Sci. 2021;7:665–92.
37. Pan WW, Wubben TJ, Besirli CG. Photoreceptor metabolic reprogramming: current understanding and therapeutic implications. Commun Biol. 2021;4(1):245.
38. Liu YV, Santiago CP, Sogunro A, Konar GJ, Hu MW, McNally MM, et al. Single-cell transcriptome analysis of xenotransplanted human retinal organoids defines two migratory cell populations of nonretinal origin. Stem Cell Reports. 2023;18(5):1138–54.
39. Eguchi N, Damyar K, Alexander M, Dafoe D, Lakey JRT, Ichii H. Anti-oxidative therapy in islet cell transplantation. Antioxidants (Basel). 2022;11(6).
40. Zeng W, Xiao J, Zheng G, Xing F, Tipoe GL, Wang X, et al. Antioxidant treatment enhances human mesenchymal stem cell anti-stress ability and therapeutic efficacy in an acute liver failure model. Sci Rep. 2015;5:11100.
41. Chang D, Park K, Famili A. Hydrogels for sustained delivery of biologics to the back of the eye. Drug Discov Today. 2019;24(8):1470–82.
42. Liu Y, Wang R, Zarembinski TI, Doty N, Jiang C, Regatieri C, et al. The application of hyaluronic acid hydrogels to retinal progenitor cell transplantation. Tissue Eng Part A. 2013;19(1–2):135–42.
43. Lee IK, Ludwig AL, Phillips MJ, Lee J, Xie R, Sajdak BS, et al. Ultrathin micromolded 3D scaffolds for high-density photoreceptor layer reconstruction. Sci Adv. 2021;7(17).
44. Lee IK, Xie R, Luz-Madrigal A, Min S, Zhu J, Jin J, et al. Micromolded honeycomb scaffold design to support the generation of a bilayered RPE and photoreceptor cell construct. Bioact Mater. 2023;30:142–53.

45. Jung YH, Phillips MJ, Lee J, Xie R, Ludwig AL, Chen G, et al. 3D microstructured scaffolds to support photoreceptor polarization and maturation. Adv Mater. 2018;30(39): e1803550.
46. Wang AL, Yu AC, Lau LT, Lee C, le Wu M, Zhu X, et al. Minocycline inhibits LPS-induced retinal microglia activation. Neurochem Int. 2005;47(1–2):152–8.
47. Yrjanheikki J, Tikka T, Keinanen R, Goldsteins G, Chan PH, Koistinaho J. A tetracycline derivative, minocycline, reduces inflammation and protects against focal cerebral ischemia with a wide therapeutic window. Proc Natl Acad Sci U S A. 1999;96(23):13496–500.

Publisher's Note